

BioTechniques®

The International Journal of Life Science Methods



MICROBIOLOGY



www.biotechniques.com



CONTENTS

OPINION

Appreciating complexity in host-microbe interactions

APPLICATION NOTE

Pressure differential evaluation of multiple linked laboratory manifolds

TECH NEWS

Metagenomics: preventing future pandemics

BENCHMARK

Triplicate PCR reactions for 16S rRNA gene amplicon sequencing are unnecessary

SCIENTIFIC BRIEF

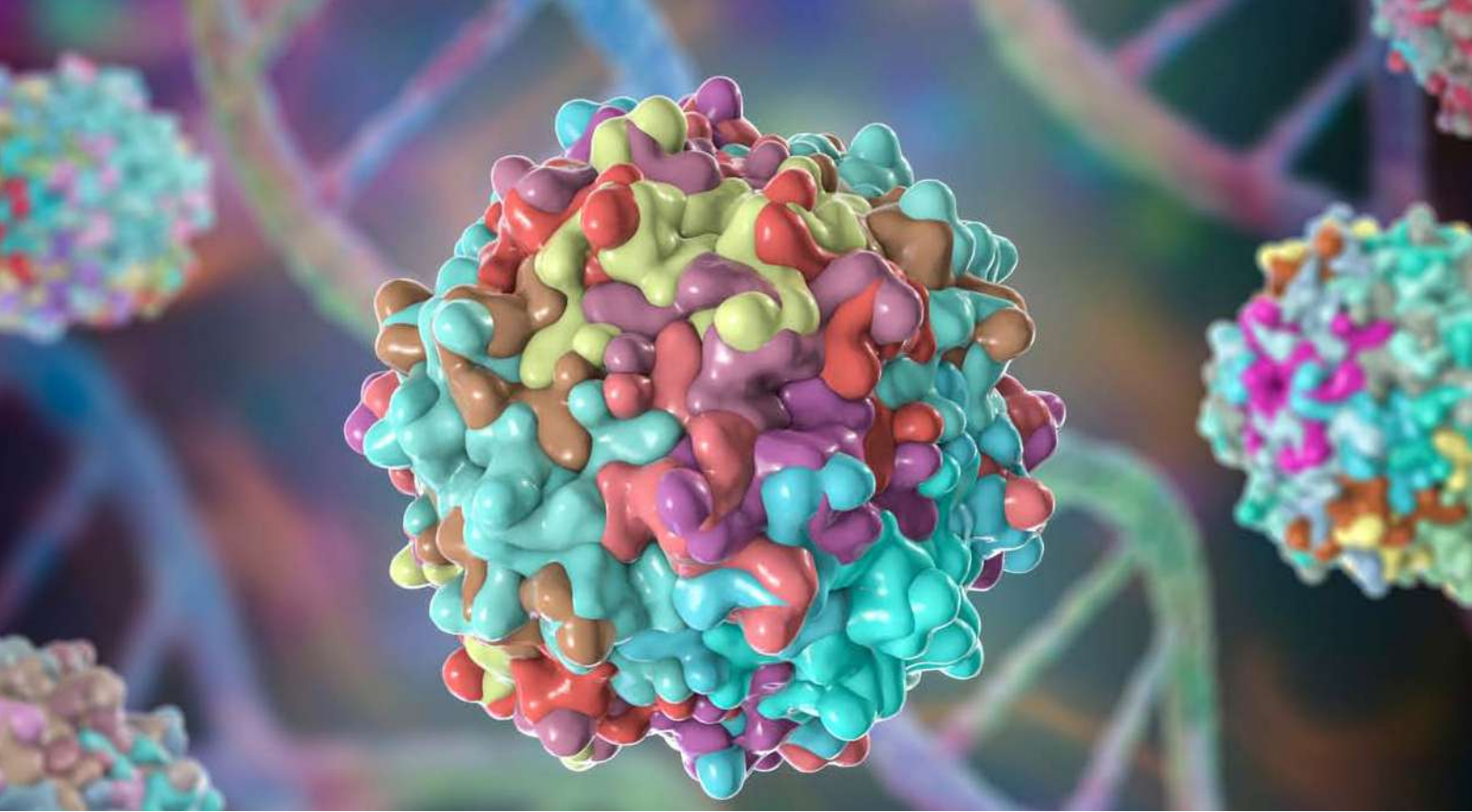
How ergonomics and cleaning ease reduce repetitive stress injuries and contamination in pharmaceutical lab workflows

REPORT

A comparison of DNA/RNA extraction protocols for high-throughput sequencing of microbial communities

REPORT

An engraved surface induces weak adherence and high proliferation of nonadherent cells and microorganisms during culture



Appreciating complexity in host-microbe interactions

We often consider host-microbe interactions as two partners each playing a role to maintain or destroy balance. But really, they are more like spider webs of interactions holding together hundreds – or even thousands – of different species. Can diving into the complexity of these relationships help us to understand the world, or do we just end up with more questions than answers?

Most people who have taken a course in microbiology are well-aware of Koch's Postulates. Published by Robert Koch in 1890, these rules of rational and deliberate testing to find out which microbe causes a certain illness laid the framework for many of modern medicine's principles and techniques. Pared down completely, the postulates require that a microbe should be found in a sick individual and should cause the disease when given to an otherwise healthy individual.

Although some of Koch's postulates have been amended (for instance, to account for asymptomatic carriers who carry the bacteria without showing signs of illness or viruses that can't be grown without a host cell), the general idea permeates microbial studies: a disease is caused by one microbe.

We love stories of clear-cut explanations, when science can find one cause for one effect. But most stories aren't quite so simple. While extremely useful, these "one microbe, one disease" parameters fail to encapsulate the complexity of how microbes interact with their host environment. As we've grown to understand over the past several decades, most environments that allow for the life of one microbe also allow for many microbes to live together.

Rather than thinking in terms of healthy or harmful microbes, we have to consider how entire microbiota (microbe communities) can affect the health of their host. In terms of bacteria, not only do the microbes interact with their host, but they communicate with each other and affect their neighbors' behaviors.

Of course, we still need to distill down our questions to create testable hypotheses. We can focus our questions while leaving our field for possibilities wide open. By asking "what is causing this disease?" rather than limiting ourselves to one microbe at a time, we can begin to understand and control how entire microbial ecosystems might be affecting human health and interests. I've highlighted three examples of how examining host-microbe interactions through the lens of complex microbial communities actually gives us more tools to find our answers.

Gingivitis

Whether you call them cavities, caries, or just tooth decay, nobody wants to have to visit a dentist because of tiny holes in our teeth or swollen gums. Usually attributed to eating too much sugar or drinking carbonated beverages, gingivitis is actually caused by species like *Porphyromonas gingivalis* leaving a slimy film called dental plaque. Great, that's pretty simple. So, let's make sure to get all of these bacteria off our teeth. With this understanding, targeting removal of *P. gingivalis* specifically seems like the best option to avoid gingivitis (other than removing all of one's teeth).

But what if I told you that these bacteria didn't stick to the teeth? Or, rather, they didn't directly stick to the teeth. What if I told you that *Porphyromonas gingivalis* attach to other bacteria like *Fusobacterium* species, who in turn attach to species of *Streptococcus* and *Actinomyces* that are directly attached to the dentin (surface of the tooth).

While this sequential association in the presence of hundreds of bacterial species is fascinating in itself, it also begs the question of whether our treatments could include assessment of the entire oral microbiome. With multiple steps and conditions for growth, we now have multiple targets for reducing cavities. Maybe we could limit the number of the *Fusobacterium* that attach to the *Actinomyces*; maybe we could find out why and how these species interact and change those dynamics; maybe we could find details about why some people deal with more tooth and gum disease than others even when they have the same habits.

C. diff infections

In the case of *Clostridium difficile* colitis (I implore you to not search for this on Google Images, as many a lunchtime seminar was ruined for me by others' presentations), the disease is directly caused by a bacterium called *C. difficile*; however, many people carry *C. difficile* without any symptoms. Interestingly, it's the absence of other members in the gut microbiome that allows *C. difficile* to take over and ravage its host's lower intestinal tract. Usually prompted by the administration of antibiotics, the normal microbiota of the intestine is wiped out – but, thanks to its uniquely hardy spore coat, *C. difficile* survives and proliferates.

Again, the presence of other microbes controls the behaviors of the pathogenic microbe. As such, scientists can look to understand why this happens and how to prevent the complete dysbiosis (breakdown of the normal balance of microbial species) rather than focusing solely on eradicating a notoriously tenacious pathogen.

For instance, transferring the stool of a healthy individual to the intestines of someone suffering from chronic *C. difficile* infections (called fecal microbiota transplants, or FMT) can restore balance to the gut and effectively cure the disease when other treatments have already failed. While we don't really understand how the native microbiome controls *C. difficile* growth or which individual bacteria might be important, the discovery that FMT can treat *C. diff* infections opens new opportunities for us to refine our tools and save lives.

Plant growth-promoting bacteria

Let's switch to an instance of using microbes for the benefit of a host; bacteria helping plants grow. A plant growth-promoting bacteria (PGPB) is defined as any bacterial species that has been found to increase the host plant's survival or growth under a certain circumstance, including during drought, or infection, or just general life as a plant. Similar to how eating yogurt containing live bacterial cultures can help a person prevent gastrointestinal irritation and improve their digestion, the presence of certain bacteria helps the plant to pull nutrients from the soil and protect themselves against another microbial invasion.

While some PGPB interactions are robust enough to be obvious under varying conditions, such as with Rhizobia and soybeans, many others are situation-dependent. For instance, my thesis work focused on understanding the interaction of plants with *Bacillus subtilis*, a very common soil bacteria that clearly improves plant growth under different laboratory conditions but fails to consistently produce equivalent effects in commercial fields.

While we could turn towards using chemicals or genetic manipulation to increase the effects of *B. subtilis* in fields, we can also appreciate the possible roles of neighboring microbes. The presence of certain bacteria will cause *B. subtilis* to grow and form structures that are especially resilient to stress and known to induce some crucial effects on plant immune systems. As such, it might be possible to identify "helper" bacteria to change the behaviors of *Bacillus* species so that their effects are great, more consistent, and ultimately more valuable for use in agricultural settings.

When considering host-microbe interactions, it may be simpler to think in terms of linear relationships wherein two partners each play a role to maintain or destroy balance. But really, it's more like a spider web of interactions holding together hundreds – or even thousands – of different species. Opening our minds to the idea, although intimidating, that we can't always distill down to two organisms allows us to better see and interpret the biological phenomena controlling our existence. This complexity is frustrating to decipher, as the interactions between the microbes and the host also rely on the interactions amongst the microbes. Having more players means more questions to ask but also more targets to study. There is no one-to-one relationship, and this isn't a bad thing.

View online at BioTechniques:

https://www.biotechniques.com/microbiology/opinion_appreciating_complexity_in_host-microbe_interactions/

Written by Susanna L Harris



Application Note

Pressure Differential Evaluation of Multiple Linked Laboratory Manifolds

*Maybelline Panta, Georgius de Haan, Dan Dalessio, and Patricia Lee
Pall Corporation, Westborough, MA*

Summary

The Membrane Filtration (MF) Technique is a method of analyzing aqueous samples for microbial content. With this method, a fluid sample is pulled through a membrane filter after which the filter is placed on growth media and incubated. Following the prescribed incubation period, colonies are counted and reviewed for appropriate morphology.

The MF Technique was introduced in the 1950s as a way to increase sensitivity by concentrating a larger volume of sample onto a membrane filter. Since its first introduction, the set-up for achieving the filtration has largely remained unchanged. In addition, the details of the set-up often are not documented, but passed from one analyst to another in training or learned by observing an assembled set-up (Figure 1). The most popular adaptation of the method involves a manifold which allows use of multiple funnels per vacuum source and waste disposal unit. With many samples to test per day, analysts are constantly looking for ways to increase their testing capacity. However, with many traditional manifolds currently out in the market, increasing testing capacity can be a challenge due to the inflexible nature of their design.

Pall's recently introduced Laboratory Manifold is uniquely designed for adaptability to the various microbial methods for aqueous solutions by MF technique. Interchangeable components and the use of coupling devices provide the ability to join multiple manifolds together. This increases testing capacity and adaptability to various methods.

In this application note we investigated how coupling up to three manifolds connected to a single vacuum source and operating the funnels simultaneously affects the membrane pressure differential and filtration time. We describe how a more readily measured property, filtration time, can be used as a substitute for the pressure differential (34 to 51 kPa) exerted on the filter membrane to demonstrate compliance with the US EPA Recognized Standard Methods for the Examination of Water and Wastewater (EPA Methods). We further describe how the coupled manifolds can be operated while remaining in compliance with the EPA methods.*

**EPA method parameters were used in the study because they are most descriptive of the differential pressures exerted across the membrane filter and can be correlated to filtration time.*

Figure 1

Typical Membrane Filtration Technique set up



Materials and Methods

The experiments were carried out using up to three coupled Laboratory Manifolds, a single filtering flask for waste, and a single vacuum pump (Pall part number 13158). Each individual manifold consisted of a 3-place Manifold Base (Pall part number 4889) with Elongated Standard Adapters (Pall part number 4959), and they were joined using Coupling Devices (Pall part number 4893). The vacuum pump was protected from possible filtrate carry-over by an in-line hydrophobic barrier filter (Pall part number 4250) inserted between the pump and the filtering flask. Vacuum pressure over the individual funnels was measured by pressure gauges incorporated in modified Elongated Standard Adapters (Figure 2). Each manifold was outfitted with one larger calibrated gauge and two smaller gauges. The readings of all gauges matched each other during use. The initial vacuum pressure delivered by the pump was set using the calibrated gauge on the most distant adaptor of the coupled manifolds and tracked on all gauges during filtration. 100 mL quantities of laboratory grade water were filtered through MicroFunnel™ ST Disposable Filter Funnels with 0.45 µm GN-6 Metrical® membrane (Pall part number 4811) at vacuum pressures set at 34 kPa or 51 kPa (10 inHg or 15 inHg). For measurements of simultaneously operated funnels, the valves for the funnels were opened in quick succession. The valves of evacuated funnels were closed to minimize air flow and pressure drop. Timing was started upon opening of the first valve to start filtration and stopped when the last of the funnels was fully evacuated. During filtration, the vacuum pressure displayed on the pressure gauges incorporated on the funnel adapters was monitored and the lowest observed vacuum pressure recorded.

Results

As shown in Table 1, MF Technique parameters are described using different terminology in the EPA Methods, ISO and ASTM. To remain in compliance, the various standards prescribe a pressure differential on the membrane of 34 to 51 kPa (EPA), 70 kPa at the source (ISO), or use of a source that can produce a reading of 67-80 kPa (ASTM). What often is not considered by these references is the difficulty in measuring the prescribed vacuum pressure and the way in which the various components of a filtration system will affect differential pressure at the membrane surface. While it may be possible to measure the vacuum pressure at the source as prescribed in the ISO and ASTM standards, for instance through use of a pressure gauge on the vacuum pump or the vacuum source, few if any set-ups will be able to provide readings over individual funnels as a measure of the differential pressure at the membrane surface.

Table 1

Membrane Filtration Technique vacuum standards

US EPA Recognized Standard Methods for the Examination of Water and Wastewater, 21st edition (9222 B.1.f.)

“For filtration, mount receptacle of filter-holding assembly on a 1 L filter flask with a side tube or other suitable device (manifold to hold three to six filter assemblies) such that a pressure differential (34 to 51 kPa) can be exerted on the filter membrane. Connect flask to a vacuum line, an electric vacuum pump, a filter pump operating on water pressure, a hand aspirator, or other means of securing a pressure differential (138 to 207 kPa). Connect a flask of approximately the same capacity between filtering flask and vacuum source to trap carry-over water.” [10-15 inHg]

International Standards Organization (ISO) (ISO 8199:2005 (E) 8.2.5.2)

“Connect the sterile filtration apparatus to a source of vacuum... Open stopcock and apply sufficient vacuum (about 70 kPa) to filter the water through the membrane.” [21 inHg]

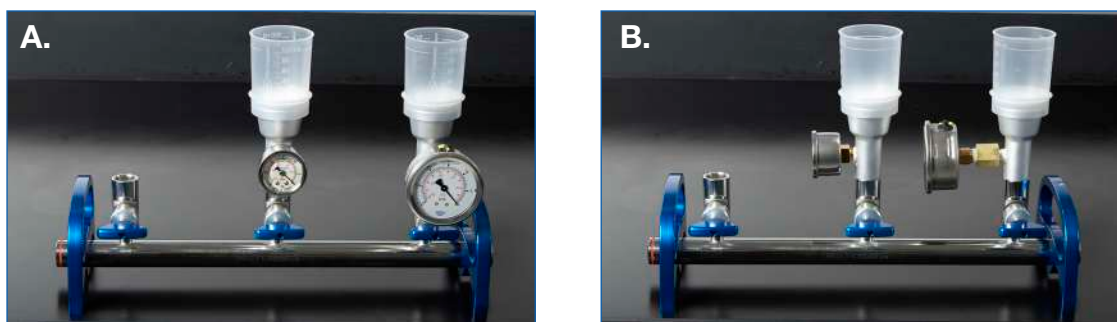
ASTM International (D 3863–87 3.2.2)

“Vacuum—for the procedure used, a source of suction that can produce a reading of 500 to 600 mm Hg on a vacuum gage.” [66.7-80.0 kPa (19.7-23.6 inHg)]

To enable tracking of the vacuum pressure differential exerted over the individual funnels during filtration, we modified Laboratory Manifolds by equipping the individual funnel adapters with pressure gauges (Figure 2). Each manifold was equipped with a single larger calibrated gauge and two smaller gauges. The readings of all gauges matched during use. Prior to filtration, the calibrated gauge on the adaptor most distant from the vacuum pump was used to set the initial vacuum pressure. During filtration, vacuum pressure was tracked on all gauges and the lowest observed vacuum pressure was recorded. As very few if any users in the field have the capability to track the vacuum pressure over the individual funnels during filtration, we also set out to measure filtration time over the individual funnels to determine if this could be used as a substitute for the vacuum pressure determinations.

Figure 2

Vacuum Manifold equipped with vacuum gauges. Frontal (A) and side (B) view of the large (calibrated) and small pressure gauges incorporated on the modified elongated standard adapters.



The results of the measurements are presented in Table 2 and Figure 3. The maximum filtration time under filtration conditions compliant with the standard methods was determined by measuring the evacuation time for a single funnel with the vacuum pressure set at 34 kPa (10 inHg), which is at the lower limit of compliance, and found an average time of 21.1 ± 1.3 s ($n = 9$). In a similar fashion, the upper limit of compliance was determined by measuring the evacuation time for a single funnel with the vacuum pressure set at 51 kPa (15 inHg). The average filtration time at this pressure was 13.9 ± 0.8 s ($n = 27$). The vacuum pressure during filtration at 34 kPa and 51 kPa (10 inHg and 15 inHg) remained stable, a clear indication that the vacuum pump had ample capacity to provide the amount of air displacement required to evacuate a single funnel without causing a pressure drop.

For measurements when simultaneously operating the three funnels on a single manifold with the vacuum pressure set at 34 kPa (10 inHg), we found that the vacuum pressure dropped to 29 kPa (8.5 inHg), below the minimum pressure threshold and observed an evacuation time of 24.5 ± 0.9 s ($n = 3$). However, filtration could be accomplished within specifications using a vacuum pressure set at 51 kPa (15 inHg). Although the vacuum pressure dropped somewhat to 47 kPa (14 inHg), this parameter remained within compliance throughout the filtration process. The average filtration time was 15.1 ± 0.7 s ($n = 3$). At the lower vacuum pressure setting of 34 kPa, the pump was unable to provide the amount of air displacement required to remain within compliance, but was able to do so when set at 51 kPa.

Referring to the EPA Methods, we reasoned that it is possible to link multiple manifolds together and operate them simultaneously only if the pressure differential across the various ports could be demonstrated to remain between 34 to 51 kPa (10 to 15 inHg). Alternatively, using the filtration time measurements with the single funnels as a guide, all funnels evacuating within a time period of 13.6 -21.0 s (95% confidence interval) could be considered compliant. The more restrictive, but easier remembered, 15 to 20 s interval could be used as a proxy. However, it should be noted that the act of opening the valves also consumes time. As shown in Table 3, valve opening times range from 1.9 ± 0.2 s for a single manifold, increasing up to 6.3 ± 0.3 s for 3 coupled manifolds ($n = 6$). These times may vary some for individual operators but should be taken into consideration especially when working with multiple coupled manifolds.

With vacuum set at 51 kPa (15 inHg), filtration with two coupled manifolds remained compliant using either specification with a lowest observed vacuum pressure differential of 44 kPa (13 inHg) and a filtration time of 17.9 ± 0.0 s ($n = 3$). When operating three coupled manifold simultaneously, filtration remained compliant, although barely, by the pressure differential standard with a lowest observed pressure differential of 34 kPa (10 inHg). Uncorrected for opening of the valves, the measured filtration time of 23.7 ± 0.5 s would appear to be out of compliance. However, taking into account the 6.3 ± 0.3 s to open the valves of the 3 coupled manifolds, filtration can be considered compliant by the time standard as well. It is clear however, that filtration of this number of funnels simultaneously puts a significant burden on the capacity of the vacuum pump. The maximum rate of filtration also is determined by set-up specific parameters such as vacuum line diameter and length and types of connectors that are used and while the set-up used in these experiments may have been compliant, other set-ups of this type might well be out of compliance.

The time standard does provide a simple way to determine if filtration takes place within compliant constraints. If more than two manifolds are coupled, operation of all simultaneously can overwhelm the capacity of the vacuum system and lead to non-compliance. However, users can use manifolds one or two units at the time even when coupling multiple manifolds and likely operate within compliance. Under these conditions, the 15-20 s filtration time interval provides an easy way to ensure compliance.

Table 2

Filtration time and minimum observed vacuum pressure during filtration. In the table, n Indicates the number of independent measurements

Number of Simultaneously Operated Funnels	Applied Vacuum Pressure							
	34 kPa (10 inHg)				51 kPa (15 inHg)			
	n	Lowest Observed Pressure (kPa)	Average Evacuation Time (s)	Std Dev	n	Lowest Observed Pressure (kPa)	Average Evacuation Time (s)	Std Dev
1	9	34	21.1	1.3	27	51	13.9	0.8
3	3	29	24.5	0.9	3	47	15.1	0.7
6	3	ND	ND	ND	3	44	17.9	0.0
9	3	ND	ND	ND	3	34	23.7	0.5

Figure 3

Minimum observed vacuum pressure and filtration times with individual funnels or with 3, 6, or 9 simultaneously operated funnels. The funnels of up to three coupled manifolds were operated individually or simultaneously and the minimum observed vacuum pressure (Panel A) and filtration times (Panel B) recorded. Vacuum pressure was set at 34 kPa or 51 kPa (10 inHg or 15 inHg). The gray bar with red upper and lower limits indicate the interval within which vacuum pressure (Panel A) or filtration time (Panel B) can be considered to be in compliance with the EPA Methods as determined from measurements with individual funnels.

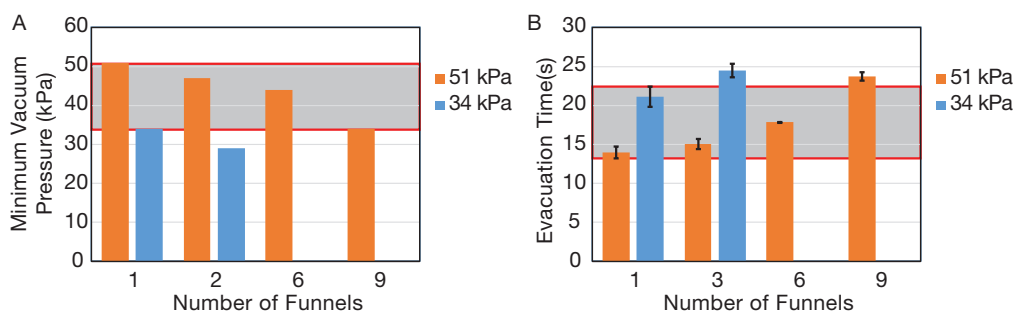


Table 3

Average valve opening times for multiple manifolds. Valve opening times reflect the average of 6 independent measurements.

Number of Manifolds	Opening Time Valves (s)	
	Average	Standard Deviation
1	1.9	0.2
2	4.0	0.2
3	6.3	0.3

Conclusions

Busy laboratories need a variety of options to accommodate testing needs. The ability to process samples in a more efficient manner often includes the need for a larger test stand. The modular design of Pall's Laboratory Manifold fulfills that need by allowing coupling of 3 port segments to create a 3-, 6-, or 9-place test stand. Operation of more than two coupled manifolds at a time may overwhelm the air displacement capacity of the vacuum source and allow the vacuum pressure to drop below the specified minimum value of 34 kPa. As it is hard to determine the vacuum pressure over individual membranes or funnels, we established that a more readily measurable parameter, filtration time, can be used instead as a substitute for the vacuum pressure. When coupling manifolds together, the funnels can be operated simultaneously as long as the filtration time takes place within 15-20 s. If this is not possible, the manifolds can be operated simultaneously as single or double units to maintain compliance with the EPA Methods.



Laboratory

Corporate Headquarters

25 Harbor Park Drive
Port Washington, New York 11050

Filtration. Separation. Solution.SM

Visit us on the Web at www.pall.com/lab

E-mail us at LabCustomerSupport@pall.com

© 2018 Pall Corporation. Pall,  Metricel, and MicroFunnel are trademarks of Pall Corporation. © indicates a trademark registered in the USA. *Filtration. Separation. Solution.* is a service mark of Pall Corporation.

METAGENOMICS: PREVENTING FUTURE PANDEMICS

Metagenomic approaches have been key to successful tracing and outbreak management during the COVID-19 pandemic. How can we use this knowledge to better prepare, strategize and prevent future pandemics?

C COVID-19 first emerged in Wuhan (Hubei, China) in December 2019 [1]. The novel coronavirus causing the disease, SARS-CoV-2, was first identified using metagenomic RNA sequencing [2] on 5 January 2020 by a team led by Zhang Yongzhen (Shanghai Public Health Clinical Center, China). On 10 January 2020, the novel coronavirus genome was posted publicly on virological.org and GenBank to assist investigations around the world [3].

COVID-19 spread rapidly amongst humans, and to other countries, leading to its classification as a pandemic by the WHO on 11 March 2020, just 2 months after the genomic information was shared. As a novel disease, there were no vaccine or targeted drugs to be used to treat or halt the spread of COVID-19, hence rapid diagnosis and isolation of patients became essential.

National lockdown, which included orders to stay and work at home, was the initial response by many countries to slow the rapid spread of the virus. Whilst this decision was met with a mixed response, it is hard to deny that this is an essential step to reduce mortality and prevent healthcare services from becoming overwhelmed.

This was supported by Flaxman *et al.*, who studied the effect of major interventions across 11 European countries for the period from the start of the COVID-19 epidemics in February 2020 until 4 May 2020, when lockdowns started to be lifted. The results indicate that major non-pharmaceutical interventions – and lockdowns in particular – have had a large effect on reducing transmission [4].

To the majority, lockdown and social distancing measures appear to be the only pandemic management strategy universally rolled out. As of 13 January 2021, there have been 92,148,761 confirmed cases of COVID-19, including 1,973,486 deaths, reported to the WHO [5]. What could have been done to keep these figures lower? Have we learned anything from previous pandemics? And, how can we prepare for future pandemics?

PROGRESS FROM PANDEMICS PAST

Few people reading this Technology News article will remember a pandemic on this scale, but history reveals that what we are currently experiencing is nothing uncommon. In the 20th century alone there have been three influenza pandemics – 1918, 1957 and 1968 (Figure 1). Promisingly, there was progression seen between these events – by 1957 there was a global network of laboratories linked to the World Influenza Research Centre in London (UK), which acted as a hub for research and virus tracking [6].

Interestingly, for all the advances made against infectious disease – health infrastructure and technology to name a few – our very growth in terms of population, migration, trade and urbanization has made us more vulnerable.

Ultimately, the goal is to detect, understand and contain infectious outbreaks at the earliest stage possible. This is fundamental in order to prevent and control outbreaks. A universal surveillance network has the potential to answer these needs.

Metagenomics is emerging as an important tool in biosurveillance, public health and clinical applications. Pandemic risk calculations employ technologies like metagenomics to trace the molecular changes in pathogens during their emergence, and mathematical models to assess risk. This combination of technologies enables us to predict an abundance of useful information – hot spots of emergence, populations at risk and the pathogens under genetic evolution.

The problem is that while the technology for surveillance is available, it is often restricted to the western hemisphere; with many diseases continuing to emerge in areas such as Southeast Asia, it is vital to ensure metagenomics and predictions of pandemic risk are shared.

Whilst this just skims the surface of previous pandemics and ideal responses, it is important to note that strides have ▶

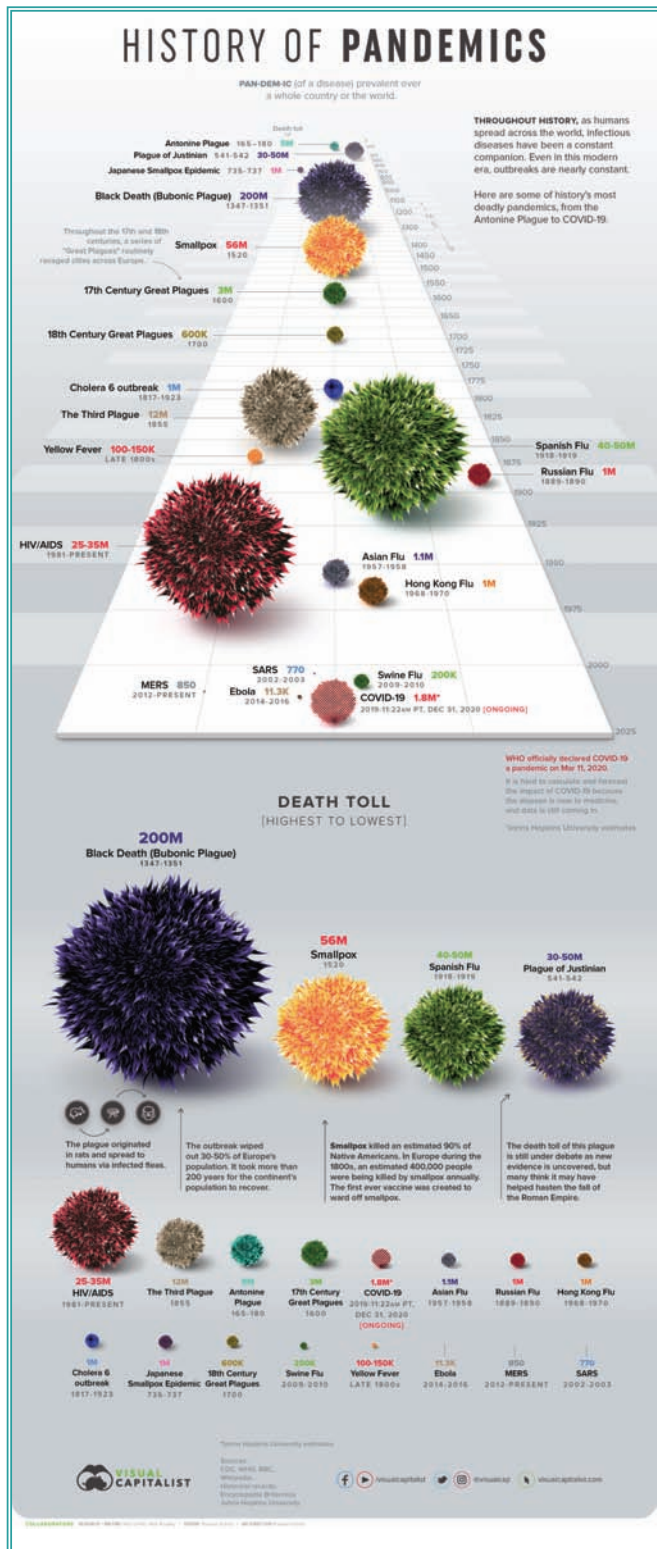


Figure 1. The history of pandemics. Reprinted from [7].

been made in terms of pandemic response; however, this piece is to highlight the potential of metagenomics in preventing a future pandemic.

HOW CAN WE DETECT A VIRUS?

Traditionally, detection of a pathogen for public health infectious disease surveillance relies upon the identification of pre-established markers of a particular disease, through assays or screening. However, through the use of next-generation sequencing (NGS), metagenomics has the ability to detect all microorganisms in a sample, regardless of whether they are known or novel pathogens [8].

There are two defined strategies through which to detect disease outbreaks. The first is syndromic surveillance, which relies on health indicators such as symptoms and patterns, before a laboratory-confirmed diagnosis is made [9]. However, this is not always an accurate method to indicate infection spread, due to the lack of a definitive disease diagnosis.

The more reliable strategy is laboratory-based surveillance, in which a number of methods can be implemented to detect and confirm pathogen presence. Within the realm of traditional pathogen detection, samples can often be left undiagnosed when there is a failure to detect a causative agent. Instead of using assays that are targeted to search for a specific pathogen, metagenomics has the potential to entirely overhaul this process, detecting the presence of all microorganisms through a single sequencing technique, and without the need for culture.

Further to this, the genomic information that can be gathered by metagenomic NGS can be used in ways beyond informing outbreak investigations, including to identify virulence genes and predict potential antibiotic resistance [8].

HOW HAVE METAGENOMICS BEEN PROPOSED TO PREVENT PANDEMICS?

The idea of using metagenomics to scan for and catch novel viruses as they arise – allowing researchers to stymie the spread of the virus early, thereby preventing the possibility of a pandemic before it has begun – is not a new one. In fact, a 2016 paper published in *PNAS* warned of a SARS-like virus “poised for human” emergence [10].

The paper highlighted WIV1-CoV, isolated from Chinese horseshoe bat populations in a previous metagenomic study (Figure 2) [11], as being of particularly high risk for emergence in humans after both chimeric and full-length zoonotic versions of the virus were shown to be capable of replicating *in vivo* in humans. Sound familiar?

The paper highlighted that – while metagenomic screens had identified that SARS-like viruses were circulating in these bat populations and that species with the potential to evolve into human infectious strains had been identified in previous studies [11] – these observations alone were not enough. Commenting on the *PNAS* paper in another article for the same issue, Vincent Racaniello (Columbia University Medical Center, NY, USA) stated that “gazing at viral sequences has its limits; experiments need to be done” [12].

The authors of the *PNAS* paper outlined an approach to take metagenomic data and examine them experimentally to determine the probability of a virus becoming infectious to humans, the likely severity of the resultant infection and our preparedness to deal with the emergent species if it does [10]. To explore the

severity and probability they conducted a series of mouse model experiments involving transgenic mice, manipulated to express the human ACE2 receptor – the receptor bound by coronavirus spike proteins.

To assess our preparedness for the emergence of WIV1-CoV into human populations, the authors tested the efficacy of antibodies generated to protect against SARS-CoV in blocking infection by WIV1-CoV, first in cell culture and then in the transgenic mouse model. This identified an antibody that did prevent replication of the virus and protect against severe disease; however, preliminary attempts to determine whether vaccines composed of inactivated SARS-CoV would be effective against WIV1-CoV proved negative [10].

Ultimately, this case study highlighted that there are viruses on the cusp of making the leap from animal to human pathogenicity, that we were not prepared for these viruses with an easily adaptable vaccine and that potential treatments for these viruses could include broadly neutralizing antibodies.

Racaniello, drawing next steps from these key points, laid out several recommendations for further study [12]. First, a study to identify a panel of antibodies effective in preventing the invasive action of the spike protein common to coronaviruses. Next, the identification of the genome alterations required for WIV1-CoV to become infectious to humans – an action that should be applied to all viruses identified as at risk of infecting humans. Finally, an examination of the mechanism by which pathogenicity of these viruses could increase.

WHAT WENT WRONG?

So, with these actions highlighted and the risk of future pandemics laid bare, what went wrong? To investigate many of these actions would have required gain-of-function experiments on these viruses. At the time of the paper's publication, there was heated debate about the risks of these experiments, with opposition occasionally citing apocalyptic scenarios worthy of Hollywood. These arguments, whilst founded on little actual evidence [13], were nonetheless captivating enough to provoke the US government to issue a moratorium severely restricting these experiments [14].

While this restriction was lifted in December 2017 [15], this period would have delayed these crucial studies and dampened the impact of this paper, perhaps preventing the recommendations of Racaniello being pursued.

Meanwhile, debate on the gain-of-function studies still rages and can perturb researchers from undertaking them, with many legitimate reservations needing to be thoroughly addressed [16] and more sensationalist articles fanning the flames of debate [17]. While the debate surrounding the topic is by no means entirely one-sided in the virology community, instead of quashing the practice, protocols need to be put in place to ensure that these studies are conducted in the safest possible manner, in an open and accountable setting – actions that may take the heat out of the debate and allow safe progress in research that that could prove invaluable. For metagenomic scanning to be worth its salt, it needs to be accompanied by the ability to follow-up the findings in an effective but safe manner.



Figure 2. A Chinese horseshoe bat. Shutterstock.com.

THE ICELANDIC APPROACH

PCR testing was quickly established as the 'gold standard' of diagnosis, allowing for scalable, rapid and comparatively cheap results, with a good level of reliability. However, there are clear benefits in combining traditional laboratory methods with metagenomic NGS to understand diseases and improve outbreak response, as has been highlighted by an open-source project, Nextstrain [18].

Globally, the primary focus during the COVID-19 outbreak was on rapid testing, not whole-genome sequencing, with some countries completely polarized in their position on metagenomic analysis for tracing SARS-CoV-2 infection.

In May 2020, a team of researchers across countries in East Africa contributed to an article for *BioTechniques* questioning where the SARS-CoV-2 genomes from East Africa were [19]. At the time of writing the article, which was published on 15 May 2020, there were no publicly available SARS-CoV-2 genomes from East Africa – more than 10 weeks after the first reported COVID-19 case in Kenya.

As outlined in the article, a French study that was listed on bioRxiv – now published in *Eurosurveillance* [20] – demonstrated through NGS analysis that the first recorded cases of COVID-19 in France were not of Chinese origin, suggesting that SARS-CoV-2 was present in the country prior. This insight is crucial for biosurveillance purposes and outbreak management.

The Icelandic approach to COVID-19 focused heavily on scientific methods, encompassing metagenomic techniques, and has been hailed as "*pivotal*" in its contribution to understanding the pandemic [21]. deCODE (Reykjavik, Iceland), a human genomics company and subsidiary of Amgen (USA), offered their services to Iceland's Directorate of Health. Together, they tracked the health of every Icelander who tested positive for SARS-CoV-2, isolated and sequenced captured

COVID-positive samples and screened more than half of the 368,000 population for infection.

They both uncovered crucial insights about COVID-19 infection, including that almost half of infected people are asymptomatic, and prevented high numbers of deaths – reporting approximately 7 per 100,000 in comparison to the USA's approximate 80 per 100,000 – while still keeping their borders open to tourists.

METAGENOMIC PROTOCOLS IN THE COVID ERA

A study published in the *Journal of Clinical Virology* in October 2020 outlined the validation of a metagenomics protocol for coronavirus identification by simulating novel virus discovery and thus, providing a potential tool for pandemic preparedness [22].

The team used clinical samples containing the coronaviruses MERS-CoV, SARS-CoV and SARS-CoV-2 to perform their metagenomic protocol. To simulate novel virus discovery, the databases they used for classification contained only known viruses prior to the discovery of these three coronaviruses.

The resultant NGS reads enabled the identification of the coronaviruses as being novel, related to the coronaviruses whose genomic information was present in the databases, validating the protocol for novel coronavirus discovery.

In June 2020, a study published in *Clinical Chemistry* also outlined the detection of SARS-CoV-2 by metagenomic analysis. The researchers evaluated laboratory-confirmed COVID-positive and -negative samples with metagenomic NGS, comparing the readouts to a genomic database from 2019, which was created prior to SARS-CoV-2 discovery [23].

Through this method, they were able to identify the novel coronavirus within 36 hours. This study did have a poor sample size; however, the benefits of metagenomic sequencing were also highlighted. The team identified numerous other viruses present in the samples, providing a less targeted diagnosis route, identifying why the patient is ill and the best course for treatment.

METAGENOMIC PROTOCOLS POST-COVID

The extent and severity of the COVID-19 pandemic has some researchers looking to the future and questioning: where might the next pandemic come from and how can it be prevented?

An article published in *Nature* in March 2020 outlined the identification of two SARS-CoV-2-related coronaviruses in Malayan pangolins through metagenomic sequencing, one of which had a receptor-binding domain incredibly similar to that of SARS-CoV-2 [24].

The researchers suggest that since the SARS-CoV-2 outbreak has been associated with a seafood market, pangolins should be removed from markets as a preventative measure for a future coronavirus outbreak.

The potential of metagenomics in detecting and tracing novel coronaviruses is immense. Although metagenomics may

be a relatively recent field, it is certainly not novel. Due to the immediate severity, rapid spread and relative lack of preparedness (in comparison to the vast knowledge that has been gained during the pandemic), there perhaps was not the time or resource to focus on metagenomic sequencing.

However, there is a successful example to be noted in the Icelandic approach. Through careful planning and strategy, combining traditional diagnostic tests with metagenomic approaches to trace the spread and find the root of COVID-19 infection, Iceland was able to contain and minimize the spread.

Written by Abigail Sawyer, Tristan Free & Joseph Martin

REFERENCES

1. Wang H, Li X, Zhang S, Wang L, Wu X, Liu J. The genetic sequence, origin, and diagnosis of SARS-CoV-2. *Eur. J. Clin. Microbiol. Infect. Dis.* 39, 1629–1635 (2020).
2. Wu F, Zhao S, Yu B *et al.* A new coronavirus associated with human respiratory disease in China. *Nature* 579, 265–269 (2020).
3. Virological.org. Novel 2019 Coronavirus Genome (Accessed 9 December 2020). <https://virological.org/t/novel-2019-coronavirus-genome/319>
4. Seth Flaxman S, Mishra S, Gandy A *et al.* Estimating the effects of non-pharmaceutical interventions on COVID-19 in Europe. *Nature* 584(7820), 257–261 (2020).
5. World Health Organisation. WHO Coronavirus Disease (COVID-19) Dashboard (Accessed 9 December 2020). <https://covid19.who.int/>
6. Jackson C. History lessons: the Asian flu pandemic. *Br. J. Gen. Pract.* 59(565), 622–623 (2009).
7. Visual Capitalist. Visualizing the history of pandemics (Accessed 9 December 2020). <https://www.visualcapitalist.com/history-of-pandemics-deadliest/>
8. Miller R, Montoya V, Gardy J, Patrick D, Tang P. Metagenomics for pathogen detection in public health. *Genome Med.* 5, 81 (2013).
9. Mandl K, Overhage J, Wagner M *et al.* Implementing syndromic surveillance: a practical guide informed by the early experience. *J. Am. Med. Inform. Assoc.* 11(2), 141–150 (2004).
10. Menachery V, Yount B Jr, Sims A *et al.* SARS-like WIV1-CoV poised for human emergence. *Proc. Natl Acad. Sci. USA* 113(11), 3048–3053 (2016).
11. Ge X-Y, Li J-L, Yang X-L *et al.* Isolation and characterization of a bat SARS-like coronavirus that uses the ACE2 receptor. *Nature* 508, 535–538 (2013).
12. Racaniello V. Moving beyond metagenomics to find the next pandemic virus. *Proc. Natl Acad. Sci. USA* 113 (11), 2812–2814 (2016).
13. The apocalypse as a rhetorical device in the influenza virus gain-of-function debate. *Mbio* 5(5), e02062–14 (2014).
14. The White House President Barack Obama. Doing diligence to assess the risks and benefits of life sciences gain-of-function research (Accessed 9 December 2020). <https://obamawhitehouse.archives.gov/blog/2014/10/17/doing-diligence-assess-risks-and-benefits-life-sciences-gain-function-research>
15. Burki T. Ban on gain-of-function studies ends. *Lancet Infect. Dis.* 18(2), 148–149 (2018).
16. Imperiale M, Casadevall A. Rethinking gain-of-function experiments in the context of the COVID-19 pandemic. *Mbio.* 11(4), e01868–20 (2020).
17. Vox. Why some labs work on making viruses deadlier – and why they should stop (Accessed 9 December 2020). <https://www.vox.com/2020/5/1/21243148/why-some-labs-work-on-making-viruses-deadlier-and-why-they-should-stop>
18. Nextstrain. Nextstrain SARS-CoV-2 resources (Accessed 9 December 2020). <https://nextstrain.org/sars-cov-2>
19. *BioTechniques*. Where are the SARS-CoV-2 genomes from East Africa? (Accessed 9 December 2020). https://www.biotechniques.com/covid-19/opinion_where-are-the-sars-cov-2-genomes-from-east-africa/
20. Gambaro F, Behillil S, Baidaliuk A. Introductions and early spread of SARS-CoV-2 in France, 24 January to 23 March 2020. *Euro. Surveill.* 25(26), 2001200 (2020).
21. *Nature*. How Iceland hammered COVID with science (Accessed 9 December 2020). <https://www.nature.com/articles/d41586-020-03284-3>
22. Carbo E, Sidorov L, Zevenhoven-Dobbe J *et al.* Coronavirus discovery by metagenomic sequencing: a tool for pandemic preparedness. *J. Clin. Virol.* 131, 104594 (2020).
23. Peddu V, Shean R, Xie H *et al.* Metagenomic analysis reveals clinical SARS-CoV-2 infection and bacterial or viral superinfection and colonization. *Clin. Chem.* 66(7), 966–972 (2020).
24. Lam T, Jia N, Zhang Y-W *et al.* Identifying SARS-CoV-2-related coronaviruses in Malayan pangolins. *Nature* 583, 282–285 (2020).

Triplicate PCR reactions for 16S rRNA gene amplicon sequencing are unnecessary

Clarisse Marotz¹, Anukriti Sharma², Greg Humphrey¹, Neil Gottel², Christopher Daum³, Jack A Gilbert², Emiley Eloë-Fadrosch³ & Rob Knight^{*1,4,5}

ABSTRACT

Conventional wisdom holds that PCR amplification for sequencing should employ pooled replicate reactions to reduce bias due to jackpot effects and chimera formation. However, modern amplicon data analysis employs methods that may be less sensitive to such artifacts. Here we directly compare results from single versus triplicate reactions for 16S amplicon sequencing and find no significant impact of adopting a less labor-intensive single reaction protocol.

METHOD SUMMARY

We compared single PCR reactions to pooled triplicate PCR reactions for 16S rRNA gene amplicon sequencing on nearly 400 samples from a diverse range of environments across three independent laboratories.

KEYWORDS

16S rRNA gene amplicon sequencing • microbiome • PCR • replicate PCR reactions

¹Department of Pediatrics, University of California, San Diego, La Jolla, CA, USA; ²Division of Bioscience, Argonne National Laboratory University of Chicago, Chicago, IL, USA; ³Department of Energy Joint Genome Institute, Walnut Creek, CA, USA; ⁴Center for Microbiome Innovation, University of California San Diego, La Jolla, CA, USA; ⁵Department of Computer Science and Engineering, University of California San Diego, La Jolla, CA, USA; *Author for correspondence: robknight@ucsd.edu

BioTechniques 67:29-32 (July 2019) 10.2144/btn-2018-0192

For decades, 16S rRNA gene sequencing has been performed by pooling replicate PCR reactions, usually in triplicate. The primary benefit is to reduce ‘jackpotting’: the stochastic nature of PCR means that some molecules are amplified earlier than others, and exponential amplification in subsequent rounds of PCR substantially distort the frequencies of different molecules in heterogeneous pools of target genes [1]. This phenomenon is particularly important in environmental DNA sequencing where the goal is an accurate, or at least consistent, readout of the different gene targets matching a primer set.

However, since the guideline that PCR should be performed in triplicate was introduced [1], there have been substantial improvements in the processivity and fidelity of DNA polymerases. Therefore, triplicate PCR may no longer provide the benefits it once did, although performing single PCR reactions instead of triplicate would provide significant time and cost savings. Several studies have tested single versus triplicate PCR for 16S rRNA sequencing in limited settings with a small number of input samples (e.g., 18 soil samples [2], two soil and two stool samples [3], three soil samples [4]). However, it has never been tested across the wide range of samples and settings that would be needed to justify a general recommendation for change in protocol. We used the availability of standardized sample sets such as those from MBQC, the Microbiome Quality Control project [5], and from our previous technology testing to answer this question definitively across three different laboratories. In total, we tested the effects of replicate PCR pooling in three independent experiments containing nearly 373 samples from a diverse range of environments.

First, we benchmarked single versus pooled-triplicate PCR across a broad range of sample types. In our previous study on comparison of DNA extraction methods [6] we assembled a set of 96 samples spanning a broad range of environments, including 48

fecal samples, 12 soil samples, 12 marine sediment samples, six seawater samples, five skin samples, five oral samples, and six mattress dust samples. We used the DNA from this previous study, extracted using the Earth Microbiome Project protocol [7] on the Kingfisher instrument, for this study. 16S rRNA gene amplification was performed according to the Earth Microbiome Project (EMP) protocol and is detailed in the supplemental file. We quantified amplicons by PicoGreen™ and pooled 240 ng of each for sequencing. We ran the entire sample set four times: twice with single PCR and twice with pooled-triplicate PCR. The pooled library was sequenced on the Illumina MiSeq sequencing platform with a MiSeq Reagent Kit v2 and paired-end 150 cycles. All data were processed and analyzed using the QIIME2 software suite [8] and Deblur [9]. Counterintuitively, single PCR reactions yielded significantly more reads than triplicate PCR reactions (mean ± SEM: 10,821 ± 298 versus 10,029 ± 262, respectively, paired T-test p = 0.0003), and fewer dropouts (Figure 1A). We saw no significant difference in alpha diversity, regardless of environment (Figure 1B). Beta diversity analysis with Unweighted UniFrac demonstrates that samples cluster by sample type and not number of PCR reactions (Figure 1C). The Weighted UniFrac distances are significantly larger among samples from different environments than among biological replicates, and distances among biological replicates are significantly greater than technical replicates, with both single and triplicate PCR reactions (Figure 1D). Negligible taxonomic changes between single and triplicate reactions were observed (97.8% shared taxonomy at the species level, genus 98.4%, and phylum 100%, Supplementary Figure 1A & Supplementary Figure 2).

Second, because high-level conclusions crossing environment types might obscure relationships in particular sample types, we tested whether the conclusions held for a separate set of agricultural ▶

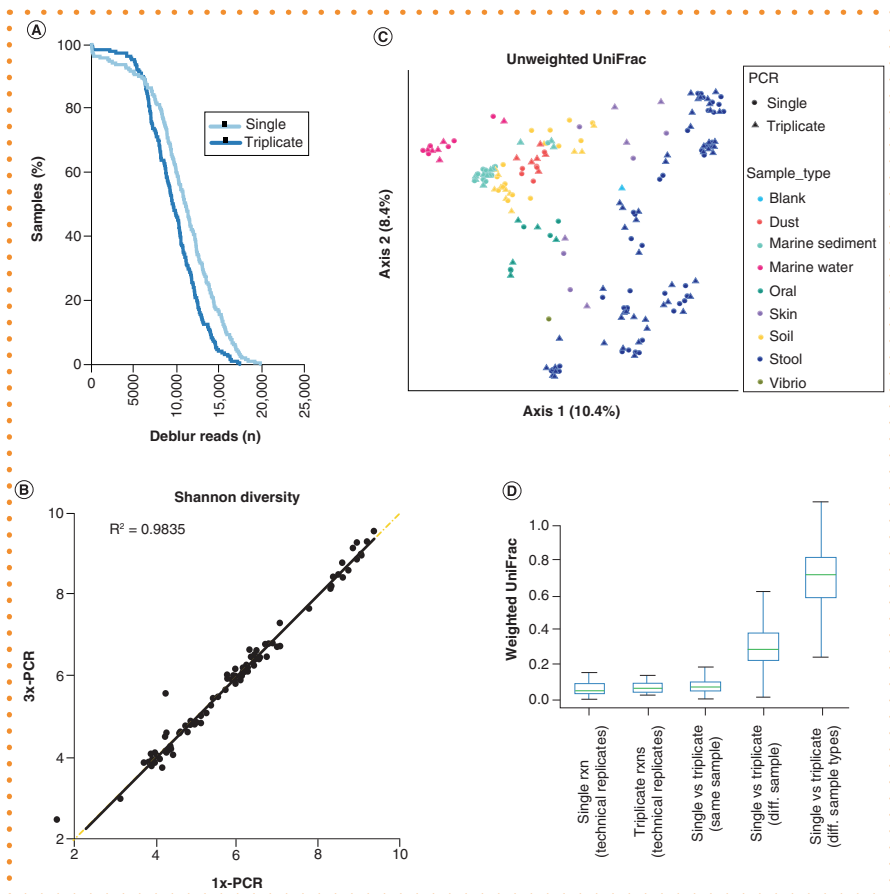


Figure 1. Effect of 16S PCR reaction number across a broad range of sample types. (A) The sequencing dropout rate of all samples run with either single or triplicate PCR reactions. (B) Shannon diversity index is nearly identical between single and triplicate PCR reactions of the same sample. (C) Unweighted UniFrac PCoA plot shows that samples cluster by sample type (color) and not number of PCR reactions (shape). (D) Weighted UniFrac distance among technical replicates (same sample) run with either single or triplicate PCR reactions are smaller than the distance between samples of the same type (diff samples) or among samples from different environments (types).

► samples. We sampled root and rhizosphere samples from three different sites across two seasons. A variety of roots including crown, seminal, and primary roots were excavated and shaken for 1–2 min in 35 ml phosphate buffer and maintained on ice. In the laboratory, roots were surface sterilized by rinsing 30 s in 5.25% sodium hypochlorite + 0.01% Tween 20, followed by a 30 s rinse in 70% ethanol, followed by three rinses in sterile ultrapure water. Roots were blotted dry on a clean paper towel, placed in a 15 ml tube, frozen at -80°C and then ground in liquid nitrogen prior to DNA extraction. The rhizosphere samples were filtered through a sterile 100 μm mesh filter, pelleted at 3000 \times g for 10 minutes, washed with 1.5 ml phosphate buffer, and re-pelleted by spinning for 5 min at full speed. The supernatant was

drained off and the rhizosphere soil pellet was stored at -80°C until DNA extraction. DNA was extracted from soil, rhizosphere, and root samples using DNeasy PowerSoil HTP 96 Kit and quantified with the QuantiFluor dsDNA reagent. Each sample was amplified both with a single PCR reaction and with pooled-triplicate reactions. The single PCR reactions yielded significantly more reads than triplicate PCR reactions (mean \pm SEM: 3631 \pm 139 versus 3000 \pm 113, respectively; paired T-test $p < 0.0001$), but had a similar dropout rate (Figure 2A). Alpha diversity was not significantly different with single versus triplicate PCR (Figure 2B), and as with the cross-environment comparison shown in Figure 1, Weighted UniFrac analysis shows that the primary clustering is by sample type and the distances among

samples does not differ in single versus triplicate PCRs (Figure 2C & D). Negligible taxonomic changes between single and triplicate reactions were observed (99.3% shared taxonomy at the species level, genus 99.2%, and phylum 100%, Supplementary Figure 1B & Supplementary Figure 3).

Finally, the microbiology of the built environment has been a rapidly expanding topic of interest over the past decade but poses unique challenges for molecular analysis. In particular, samples tend to be contaminated with high levels of human DNA and have low bacterial biomass [10]. We used samples from a previous study that collected 96 samples longitudinally from four commonly used building materials maintained at a high relative humidity ($\sim 94\%$) [11]. Genomic DNA was extracted from environmental samples using the PowerSoil DNA isolation kit as previously described [12], and genomic DNA was amplified using the EMP protocol as detailed in the supplemental file. Samples were processed both with single PCR and pooled-triplicate PCR reactions, and sequenced on an Illumina MiSeq sequencing platform with a MiSeq Reagent Kit v2 and paired-end 150 cycles. Once again, yields were higher with single PCR than triplicate PCR (Figure 3A), Shannon diversity was not affected by single versus triplicate PCR (Figure 3B), and beta diversity was driven by biological parameters of the sample rather than by single versus triplicate PCR (Figure 3C & D). Negligible taxonomic changes between single and triplicate reactions were observed (96.5% shared taxonomy at the species level, genus 95.8%, and phylum 100%, Supplementary Figure 1C & Supplementary Figure 4). All data from each of the three experiments are publicly available from the EBI under accession number ERP113817.

Taken together, these results demonstrate that with modern methods pooling triplicate PCR reactions for 16S rRNA amplicon sequencing is more expensive and does not provide improvement over single PCR reactions. This result was confirmed in studies spanning three laboratories, hundreds of samples, and numerous distinct environment types. However, although these results hold true for the range of conditions tested here, there are so many variations in PCR techniques that this type of benchmarking effort should be

validated for specific sample types and PCR protocols before a switch from established procedure is implemented for specialized protocols. For the general sample types tested here, we recommend using single PCR reactions rather than triplicate PCR reactions. Combined with other technical improvements in miniaturizing PCR reactions [13], this change in protocol will substantially reduce the cost and complexity of amplicon studies.

AUTHOR CONTRIBUTIONS

RK, JG, and EE designed the experiments, GH, NG, and CD ran the experiments, CM and AS analyzed the data, and RK and CM wrote the manuscript.

FINANCIAL & COMPETING INTERESTS DISCLOSURE

Data from JGI was collected with support from a grant from the Office of Science (BER), US Department of Energy, Grant no DE-SC0014395 to Daniel Schachtman and Susannah Tringe. The work conducted by the US Department of Energy Joint Genome Institute, a DOE Office of Science User Facility, is supported under Contract No. DE-AC02-05CH11231. Clarisse Marotz was supported by NIDCR F31 Fellowship 1F31DE028478. The authors have no other relevant affiliations or financial involvement with any organization or entity with a financial interest in or financial conflict with the subject matter or materials discussed in the manuscript apart from those disclosed.

No writing assistance was utilized in the production of this manuscript. ▶

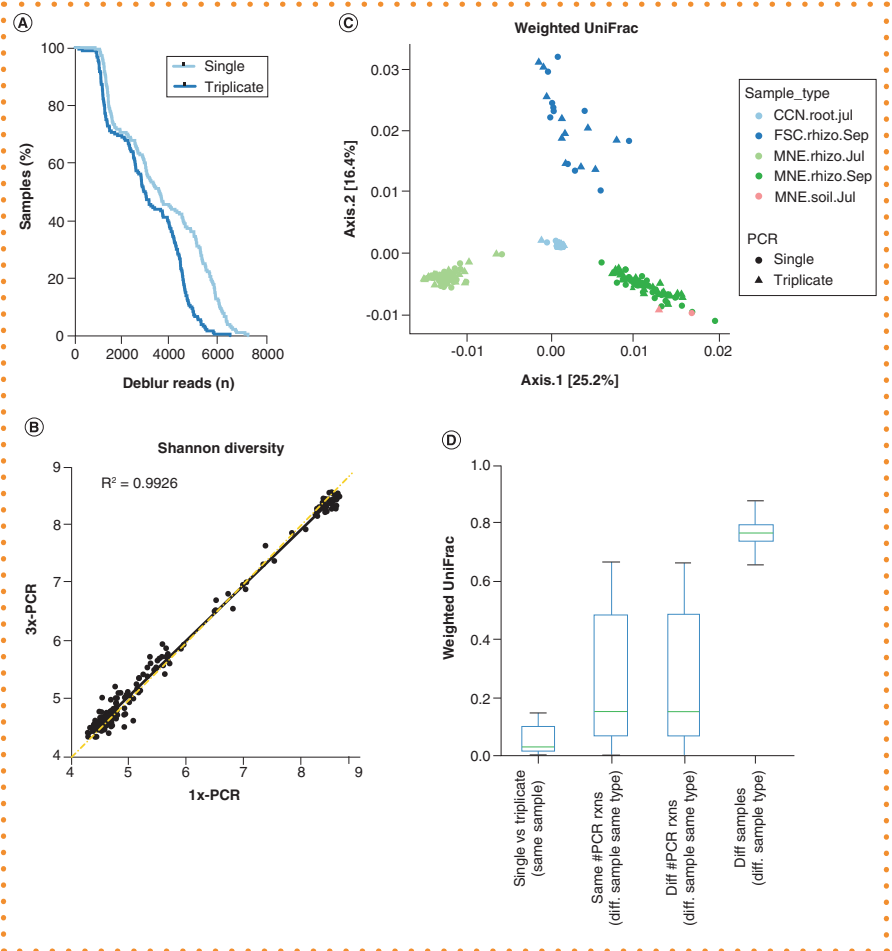


Figure 2. Effect of 16S PCR reaction number across agricultural samples. (A) The sequencing dropout number of all samples run with either single or triplicate PCR reactions. (B) Shannon diversity index of each sample is similar between single and triplicate PCR reactions. (C) Weighted UniFrac PCoA plot shows that samples cluster by sample type (color) and not number of PCR reactions (shape). (D) Weighted UniFrac distances between single or triplicate PCR reactions of the same sample are smaller than the distance between different samples of the same type run with either single or triplicate PCR reactions, and both are smaller than the distance between samples from different environments.

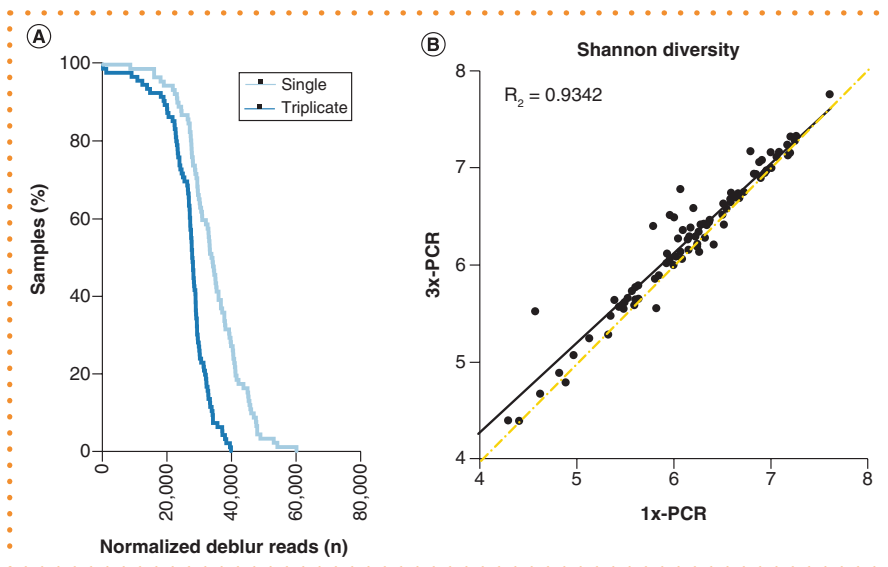


Figure 3. Effect of 16S PCR reaction number across building materials. (A) The sequencing dropout number of all samples run with either single or triplicate PCR reactions. (B) Shannon diversity index is similar between single and triplicate PCR reactions. (C) Weighted UniFrac PCoA plot shows that samples do not cluster by number of PCR reactions (shape). (D) Weighted UniFrac distances between single or triplicate PCR reactions of the same sample are smaller than the distance between different samples with either single or triplicate PCR reactions.

See overleaf for Figure 3C & D

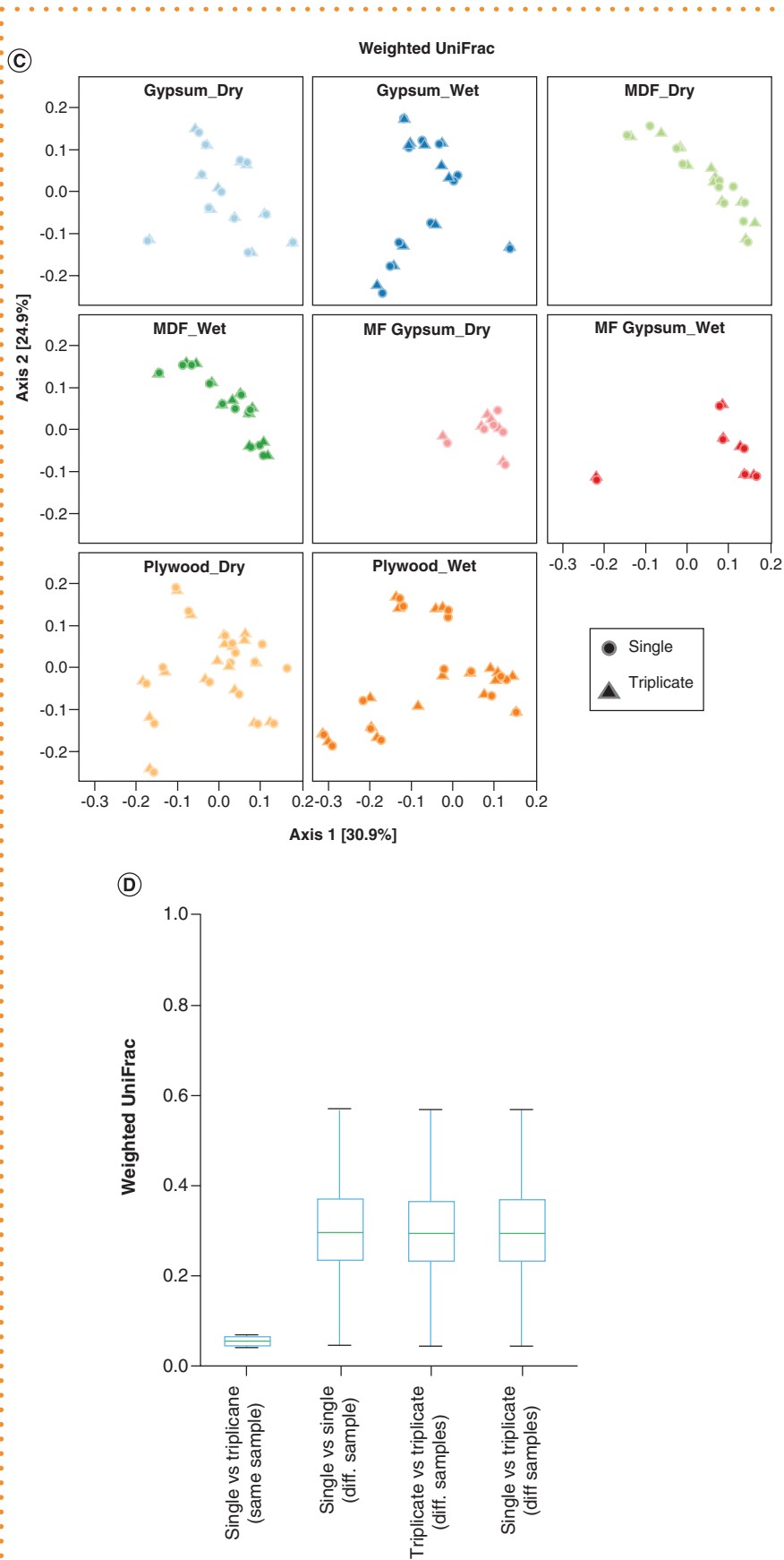


Figure 3 (cont.). Effect of 16S PCR reaction number across building materials. (A) The sequencing dropout number of all samples run with either single or triplicate PCR reactions. (B) Shannon diversity index is similar between single and triplicate PCR reactions. (C) Weighted UniFrac PCoA plot shows that samples do not cluster by number of PCR reactions (shape). (D) Weighted UniFrac distances between single or triplicate PCR reactions of the same sample are smaller than the distance between different samples with either single or triplicate PCR reactions.

► OPEN ACCESS

This work is licensed under the Attribution-NonCommercial-NoDerivatives 4.0 Unported License. To view a copy of this license, visit <http://creativecommons.org/licenses/by-nc-nd/4.0/>

SUPPLEMENTARY DATA

To view the supplementary data that accompany this paper please visit the journal website at: www.future-science.com/doi/suppl/10.2144/btn-2018-0192

REFERENCES

- Polz MF, Cavanaugh CM. Bias in template-to-product ratios in multitemplate PCR. *Appl. Environ. Microbiol.* 64(10), 3724–3730 (1998).
- Wen C, Wu L, Qin Y *et al.* Evaluation of the reproducibility of amplicon sequencing with Illumina MiSeq platform. *PLoS One* 12(4), e0176716 (2017).
- Kennedy K, Hall MW, Lynch MDJ, Moreno-Hagelsieb G, Neufeld JD. Evaluating bias of illumina-based bacterial 16S rRNA gene profiles. *80(18)*, 5717–5722 (2014).
- Smith DP, Peay KG. Sequence depth, not PCR replication, improves ecological inference from next generation DNA sequencing. *PLoS One* 9(2), e90234 (2014).
- Sinha R, Abu-Ali G, Vogtmann E *et al.* Assessment of variation in microbial community amplicon sequencing by the microbiome quality control (MBQC) project consortium. *Nat. Biotechnol.* 35(11), 1077 (2017).
- Marotz C, Amir A, Humphrey G, Gaffney J, Gogul G, Knight R. DNA extraction for streamlined metagenomics of diverse environmental samples. *Biotechniques* 62(6), 290–293 (2017).
- Gilbert J, Jansson J, Knight R. The earth microbiome project. (2010). www.earthmicrobiome.org
- Bolyen E, Rideout JR, Dillon MR *et al.* QIIME 2: reproducible, interactive, scalable, and extensible microbiome data science. No. e27295v1. *Peer J. Preprints* (2018).
- Amir A, McDonald D, Navas-Molina JA *et al.* deblur rapidly resolves single-nucleotide community sequence patterns. *mSystems* 2(2), e00191–16 (2017).
- Kelley ST, Gilbert JA. Studying the microbiology of the indoor environment. *Genome Biol.* 14(2), 202 (2013).
- Cardona C, Lax S, Larsen P *et al.* Environmental sources of bacteria differentially influence host-associated microbial dynamics. *MSystems* 3(3), e00052–18 (2018).
- McPherson MR, Wang P, Marsh EL, Mitchell RB, Schachtman DP. Isolation and analysis of microbial communities in soil, rhizosphere, and roots in perennial grass experiments. *J. Vis. Exp.* (137), e57932 (2018).
- Minich JJ, Humphrey G, Benitez RAS *et al.* High-throughput miniaturized 16S rRNA amplicon library preparation reduces costs while preserving microbiome integrity. *mSystems* 3(6), e00166–18 (2018).

How Ergonomics and Cleaning Ease Reduce Repetitive Stress Injuries and Contamination in Pharmaceutical Lab Workflows

Introduction

The repetitive nature of routine laboratory work puts pharmaceutical technicians and scientists at risk for repetitive strain injuries (RSI). Routine activities often include repeat of the same movements over and over, which can take a toll on hands, wrists, and shoulders and can lead to serious injury. According to the Occupational Safety and Health Administration (OSHA), RSI in the workplace resulted in over 300,000 cases as far back as 2015.¹

RSI is closely related to ergonomics of instrument operation when conducting simple but repetitive laboratory processes. According to an article on common laboratory worker disorders by certified ergonomist Kevin Costello, musculo-skeletal movements involving repetition, contact stress, force, and awkward posture present the most risk for injury.²

RSI can lead to laboratory user fatigue and variability that causes poor technique, errors, and cross contamination. The result is retesting that can add up to 14 days for procedures such as sterility testing. In addition, the societal costs of carpal tunnel syndrome, a key result of RSI, has been estimated at \$30,000 per case. This figure does not include indirect costs, such as lost productivity and quality of life issues that extend to everyday activities.³

Microbial cross contamination also can result when laboratory filtration devices such as manifolds, filter funnels, and pumps are difficult to clean.

This paper explores new filtration designs that are considerably more ergonomic and easier to clean than conventional products.

Reducing RSI: The Secret Is In Product Design

In a pharmaceutical microbiology laboratory, there are many ways to avoid manual labor stress by working in a more ergonomic manner. Choosing the right tools can make all the difference. Pre-sterilized filter funnels are a more efficient option for microbial contamination and quality-control testing, with the funnel and membrane in a ready-to-use, disposable system. The membrane is contained within the funnel for filtration, limiting handling and transfer, which reduces repetitive laboratory motions.

On most of these disposable devices the funnel top is removed by twisting or other motions that can put stress on wrists and arms. Additionally, twisting the top of the funnel can often tear the delicate membranes beneath, resulting in the need for retesting. When using an alternative such as the Pall MicroFunnel™ filter funnel, the top is removed with a simple squeeze of its sides. Then, the user can easily access the membrane.





Another step forward in reducing RSI is a better-designed manifold, such as the Pall Laboratory Manifold.



The Pall Laboratory Manifold has few parts, no required tools, and simple friction fittings for easy disassembly and reassembly. This simplified design can save precious time and reduce RSI risk.



Additionally, since the device's end cap and hose barb can be setup in either orientation, all the valves are situated at the front of the manifold. This means there is no need to reach over the top of a filter funnel and maneuver behind a manifold to turn the valves on and off. Both features improve contamination prevention and reduce injury risk.



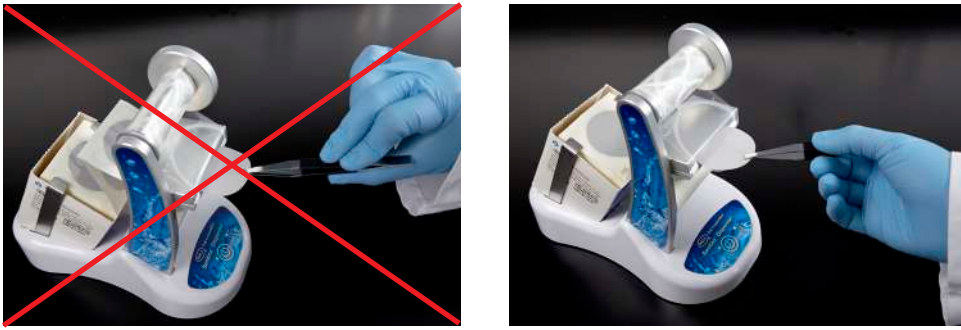
Finally, the Pall Laboratory Manifold enables processing of up to six samples at one time when two manifolds are connected together with a coupling device. Over time, this design can mean less handling and lower risk of RSI.

Reducing RSI: Improving Laboratory Techniques

RSI can be further reduced when technicians are well-trained in techniques such as the use of forceps and membrane handling. Proper orientation and handling of forceps is not only important to the technician's health, but also crucial for good microbial growth.

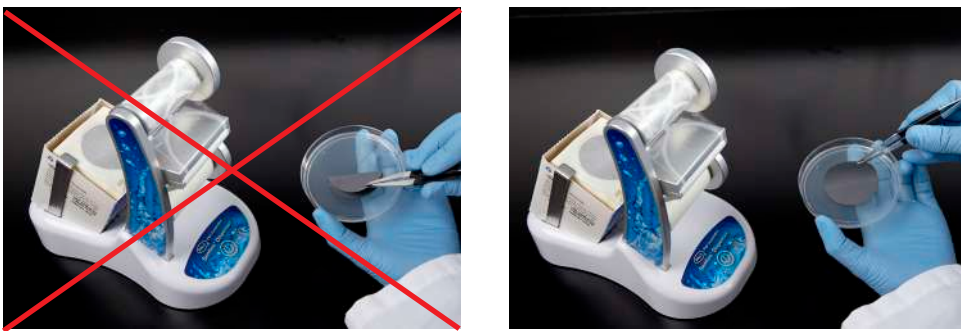
In the figures below, you can see in the left image that the hand is in an awkward position. This can cause pain during membrane removal. In the right image, the forceps are held properly, giving the hand more freedom and a more natural and comfortable feel.

Figure 1



In figure 2, the plating technique in the left image is not only awkward, but also increases the risk of creating bubbles on the bottom of the filter membrane. Air bubbles are a concern because when the agar media does not properly touch the membrane, nutrients do not reach the membrane as expected. This can cause improper cell growth that can result in false negatives. Proper technique is demonstrated in the image on the right.

Figure 2



Cleanliness: The Key to Eliminating Cross Contamination

The cleanliness of your laboratory equipment is the key to eliminating cross contamination and the resulting delays caused by retesting. Employing manifolds, pumps and funnels with easy-to-clean or disposable designs will result in contamination-free devices - a welcome advantage when cleaning is required at least once daily in high-throughput labs.

Laboratory manifolds offer microbes welcome places to hide. Look for stainless steel devices with few pieces to disassemble and assemble such as the Pall Laboratory Manifold. Their fluid paths should be free of O-rings, plus lowered hose outlets will eliminate the back-burping that can require expensive and time-consuming retesting. Make sure the manifold is designed to easily fit in laboratory autoclaves by separating into manageable components.

When purchasing a new microbiology pump, such as Pall's Sentino® pump, make sure it has a disposable fluid path that requires no cleaning or disinfection. A disposable pump fluid path, combined with a gamma-irradiated filter funnel option, virtually eliminates the risk of cross contamination from test equipment.

Disposable filter funnels, such as the Pall MicroFunnel ST filter funnels, not only eliminate cross-contamination that can come from reusable funnels, but also have a second overpack layer that streamlines cleanroom or hood entry, with one wipe down for multiple individually-packed funnels. This overpack layer reduces gross particulate contamination that can come from cardboard.

Conclusion

RSI and ease of cleaning are often overlooked when choosing the microbiology filtration solution to best suit your pharmaceutical laboratory needs. It is important to select high-performance products with ergonomics that reduce long-term injury risk. The goal is to eliminate the user fatigue and variability that can lead to poor technique, errors, and retesting. Reducing microbial cross-contamination and subsequent retesting will save the laboratory time, resources, and product development delays.

References

- 1 <https://www.bls.gov/news.release/osh2.nr0.htm>
- 2 Repetitive Strain Injury in the Laboratory, VistaLab Technologies, August 25, 2020.
- 3 Repetitive Strain Injury in the Laboratory, Biocompare, March 29, 2018.



Corporate Headquarters
Port Washington, NY, USA
+1-800-717-7255 toll free (USA)
+1-516-484-5400 phone

European Headquarters
Fribourg, Switzerland
+41 (0)26 350 53 00 phone

Asia-Pacific Headquarters
Singapore
+65 6389 6500 phone

Visit us on the Web at www.pall.com/lab
Contact us at www.pall.com/contact

Pall Corporation has offices and plants throughout the world. To locate the Pall office or distributor nearest you, visit www.pall.com/contact.

The information provided in this literature was reviewed for accuracy at the time of publication. Product data may be subject to change without notice. For current information consult your local Pall distributor or contact Pall directly.

© Copyright 2021, Pall Corporation. Pall, , MicroFunnel, and Sentino are trademarks of Pall Corporation. ® Indicates a trademark registered in the USA.

A comparison of DNA/RNA extraction protocols for high-throughput sequencing of microbial communities

Justin P Shaffer¹ , Clarisse Marotz¹, Pedro Belda-Ferre¹, Cameron Martino^{1,2,3}, Stephen Wandro^{2,6}, Mehrbod Estaki¹ , Rodolfo A Salido¹, Carolina S Carpenter², Livia S Zaramela¹, Jeremiah J Minich⁴, MacKenzie Bryant¹, Karenina Sanders¹, Serena Fraraccio^{2,6}, Gail Ackermann¹, Gregory Humphrey¹, Austin D Swafford², Sandrine Miller-Montgomery^{2,6} & Rob Knight^{*1,2,5,6}

¹Department of Pediatrics, University of California, San Diego, La Jolla, CA, USA; ²Center for Microbiome Innovation, University of California, San Diego, La Jolla, CA, USA; ³Bioinformatics & Systems Biology Program, University of California San Diego, La Jolla, CA, USA; ⁴Marine Biology Research Division, University of California, San Diego, La Jolla, CA, USA; ⁵Department of Computer Science & Engineering, University of California, San Diego, La Jolla, CA, USA; ⁶Micronoma Inc., San Diego, CA, USA; *Author for correspondence: robknight@eng.ucsd.edu

BioTechniques 70: 149–159 (March 2021) 10.2144/btn-2020-0153

First draft submitted: 24 October 2020; Accepted for publication: 4 January 2021; Published online: 29 January 2021

ABSTRACT

One goal of microbial ecology researchers is to capture the maximum amount of information from all organisms in a sample. The recent COVID-19 pandemic, caused by the RNA virus SARS-CoV-2, has highlighted a gap in traditional DNA-based protocols, including the high-throughput methods the authors previously established as field standards. To enable simultaneous SARS-CoV-2 and microbial community profiling, the authors compared the relative performance of two total nucleic acid extraction protocols with the authors' previously benchmarked protocol. The authors included a diverse panel of environmental and host-associated sample types, including body sites commonly swabbed for COVID-19 testing. Here the authors present results comparing the cost, processing time, DNA and RNA yield, microbial community composition, limit of detection and well-to-well contamination between these protocols.

ACCESSION NUMBERS

Raw sequence data were deposited at the European Nucleotide Archive (accession number ERP124610), and raw and processed data are available at Qiita (study identifier 12201). Processing and analysis code is available on GitHub (https://github.com/justinshaffer/Extraction_test.Mag_MAX).

METHOD SUMMARY

To allow for downstream applications involving RNA-based organisms such as SARS-CoV-2, the authors compared the two extraction protocols designed to extract DNA and RNA with the authors' previously established protocol for extracting only DNA for microbial community analyses. Across ten diverse sample types, one of the two protocols was equivalent or better than the authors' established DNA-based protocol. The authors' conclusion is based on per-sample comparisons of DNA and RNA yield, number of quality sequences generated, microbial community alpha- and beta-diversity and taxonomic composition, limit of detection and extent of well-to-well contamination.

KEYWORDS:

16S rRNA • DNA extraction • high-throughput sequencing • limit of detection • microbial community • microbiome • RNA extraction • shotgun metagenomics • well-to-well contamination

Our growing understanding of microbial communities continues to reveal knowledge important for fostering human and environmental sustainability [1–4]. Nearly every day, new links are made between the human microbiome and human health [5–7], and the development of methods related to studying microbial communities is ever-expanding [8–10]. One major roadblock to studying microbial communities is that single methods rarely capture information from all organisms in a sample or from across diverse sample types [11–13].

The ongoing COVID-19 pandemic driven by SARS-CoV-2 has infected over 40 million human individuals and killed 1.1 million (as of 18 October 2020) [14]. Such an event represents an invaluable opportunity to study the effects of a novel pathogen on microbial interactions relevant to human hosts and other ecosystems [15–17]. Currently, the authors' protocol benchmarked for high-throughput microbiome sequencing focuses on extracting high-quality DNA from samples [18] and therefore will not capture RNA-based genomes such as that of SARS-CoV-2, which is a positive-sense, single-stranded RNA virus [19].

Here the authors aim was to identify an extraction protocol that extracts high-quality RNA while also producing DNA output and community composition comparable to the authors' previously benchmarked protocol [18]. The authors also considered technical differences

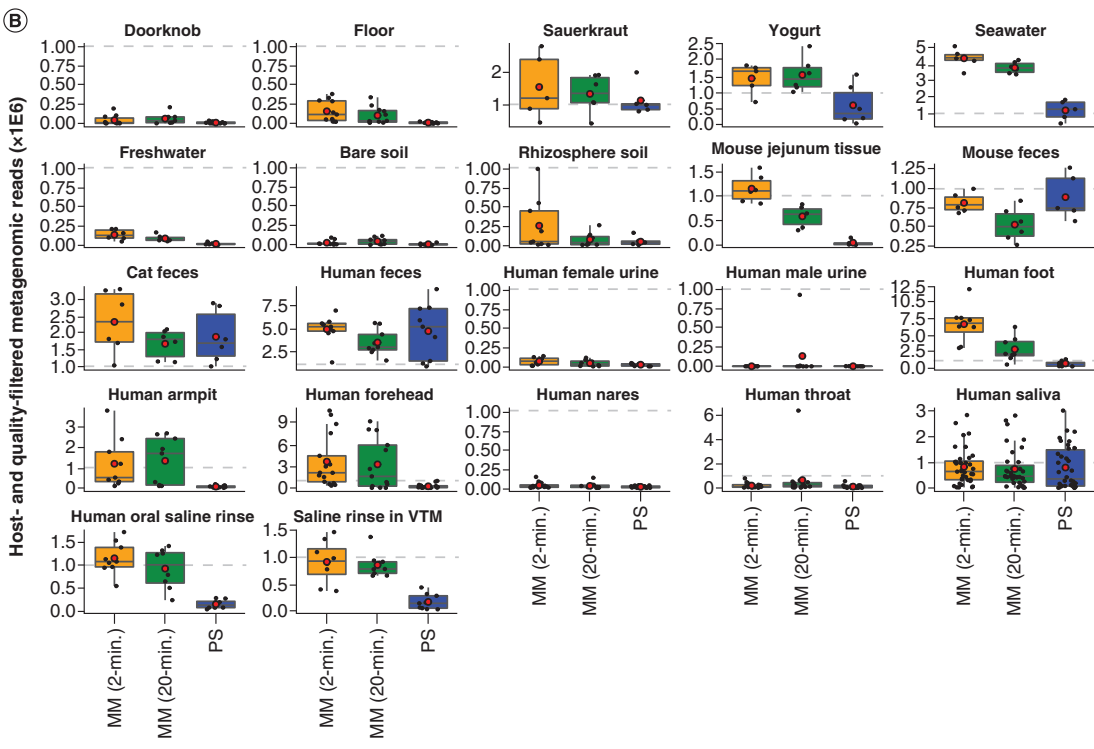
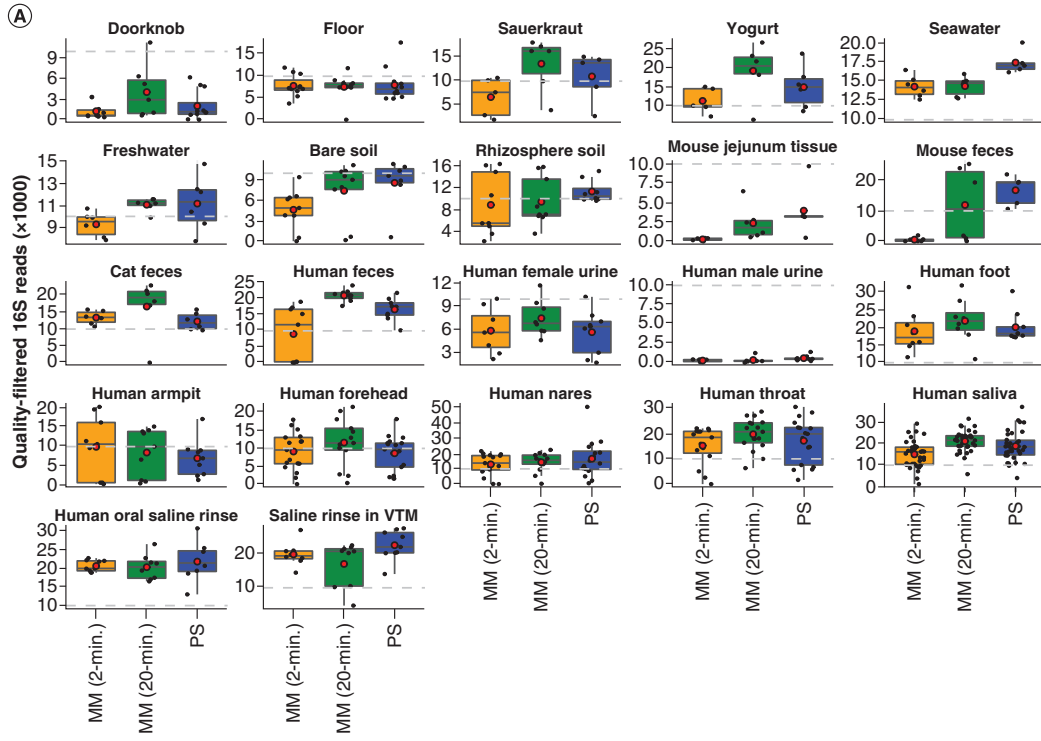


Figure 1. Sequences per sample across extraction protocols and sample types. Average number of quality sequences for (A) 16S and (B) metagenomics data ($n = 660$ samples included). Red circles indicate means. Dashed lines indicate our expectation of (A) 10,000 from 16S and (B) 1 million reads from metagenomics, respectively, for human fecal samples. Note that additional samples included here absent from our statistical test ($n = 45$) include those for which technical replication across protocols was not feasible due to recommended sampling protocols (e.g., human nares, human throat), so we included biological replicates instead. Sample types missing here lacked representation by both MagMAX protocols. MM: MagMAX; PS: PowerSoil.

Table 1. Limit of detection across extraction protocols.

Extraction protocol	Sample set	Threshold (%)	LOD		LOD mixed culture	Read depth	Samples retained	Samples retained (%)
			Gram-negative	Gram-positive				
MagMAX 2-min	High biomass	50	–	–	5.73E+02	362	76	80
		80	–	–	5.73E+04	1392	69	73
		90	–	–	5.73E+04	3512	64	67
		95	–	–	5.73E+06	9144	46	48
	Low biomass	50	1.60E+03	3.10E+03	–	637	69	73
		80	1.60E+04	3.10E+03	–	1631	63	66
		90	1.60E+04	3.10E+03	–	3007	59	62
		95	1.60E+05	3.10E+04	–	5526	52	55
MagMAX 20-min	High biomass	50	–	–	5.73E+05	8499	68	71
		80	–	–	5.73E+07	14,522	55	57
		90	–	–	5.73E+07	20,158	30	31
		95	–	–	5.73E+07	27,541	3	3
	Low biomass	50	1.60E+01	3.10E+01	–	491	79	83
		80	1.60E+03	3.10E+03	–	776	71	75
		90	1.60E+03	3.10E+03	–	1031	68	72
		95	1.60E+04	3.10E+03	–	1354	64	67
PowerSoil	High biomass	50	–	–	5.70E+01	1050	87	92
		80	–	–	5.73E+07	14,632	36	38
		90	–	–	NA	106,110	0	0
		95	–	–	NA	944,308	0	0
	Low biomass	50	1.60E+03	3.10E+00	–	1836	69	72
		80	1.60E+04	3.10E+02	–	3797	62	65
		90	1.60E+05	3.10E+03	–	5997	57	59
		95	1.60E+05	3.10E+03	–	9345	40	42

Titration of cultured cells were used to identify the number of reads needed per sample to meet various thresholds of detection (i.e., percentage of reads mapped to expected taxa vs background contaminants). Read depths corresponding to a threshold of 50% were used for filtering samples prior to community analyses of microbial 16S data, as recommended [20]. Retention of samples following filtering based on read depth for each threshold is shown.
 Gram+: *Bacillus subtilis*; Gram–: *Paracoccus denitrificans*; Mixed culture: *B. subtilis* and *P. denitrificans*; NA: Not applicable.

regarding the detection ability [20] and extent of contamination [21–23] among protocols. The authors compared DNA and RNA yield, number of quality sequences, microbial community alpha- and beta-diversity and taxonomic composition, limit of detection (LOD) and extent of well-to-well contamination across common sample types and among three extraction protocols.

Methods

Sample collection

To compare extraction protocols, the authors collected biological materials from a broad range of human and environmental samples, focusing on types widely used in studies of microbial communities and SARS-CoV-2 detection [18,24,25]. Each unique sample was aliquoted across extraction plates for comparison of extraction efficiency among protocols. The authors included a total of 33 human skin samples, 30 human oral samples, eight built environment samples, six fecal samples, six human urine samples, six soil samples, four water samples, four fermented food samples and two tissue samples. The authors collected most sample types using wooden handle cotton swabs (Puritan, CA, USA) following the standard Earth Microbiome Project protocol [26]. To make comparisons relevant to SARS-CoV-2 detection, the authors collected additional samples, mimicking those collected from patients, using BBL CultureSwab plastic handle polyester swabs (category number 220135; BD Biosciences, NJ, USA) following the CDC’s specimen collection guidelines [24,25].

The authors collected samples to allow for technical replication across three extraction protocols. Human skin samples included those from the foot, armpit, forehead and nostril interior. Foot and armpit samples were collected from three individuals by rubbing five cotton swabs simultaneously on the sole of each foot or armpit for 30 s. Forehead and nostril samples were collected from 12 individuals by rubbing two polyester swabs over the forehead for 30 s or in each nostril for 15 s each. Human oral samples included throat, saliva and oral saline rinses and the same rinses diluted in viral transport medium [27]. Throat samples were collected from 12 individuals by rubbing two polyester swabs across the pharynx for 30 s. Saliva was collected from 12 individuals using active spitting into a 50-ml centrifuge tube. Saline rinses were collected from three individuals by swishing 10 ml 0.9% saline for 30 s and spitting into a 50-ml centrifuge tube. To mimic storage in viral transport medium, 5 ml of saline rinse was mixed with 100 µl 50× viral transport medium in a 15-ml centrifuge tube. Built environment samples included floors and door handles. Floor and door handle samples were collected from two rooms using

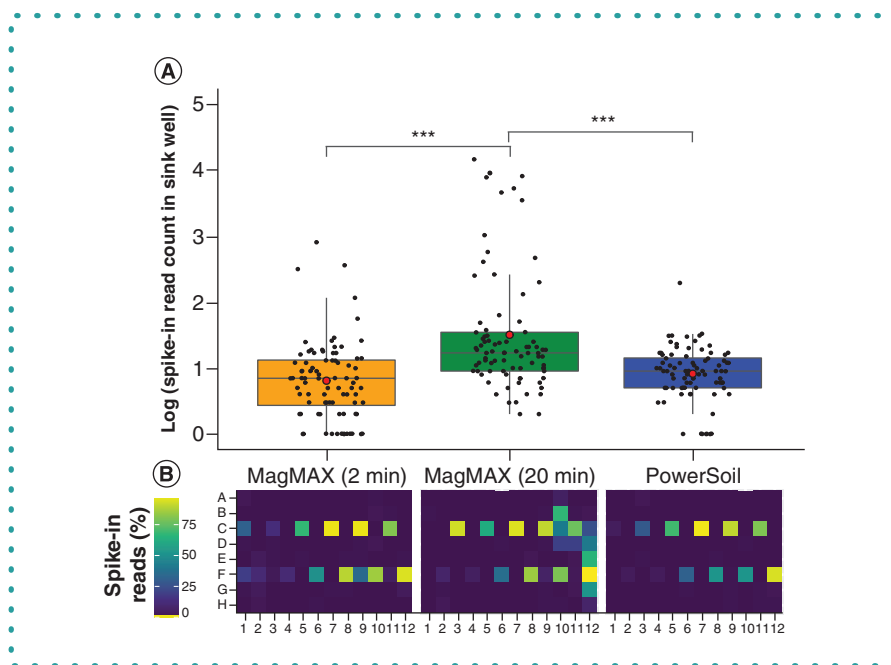


Figure 2. Well-to-well contamination across extraction protocols. Plasmids harboring synthetic 16S sequences were spiked into a single well per plate column (i.e., alternating from row C to F across columns: C1, F2, C3, F4, etc.) of each high-biomass sample plate prior to extraction. (A) The number of reads matching synthetic 16S sequences was quantified for all wells that did not receive a spike-in. Asterisks indicate significant differences between pairs of extraction protocols as determined by a Kruskal-Wallis post-hoc Dunn's test with a Benjamini-Hochberg correction for multiple comparisons. (B) The percentage of spike-in reads among all reads per well shown as a heatmap.

*** $p < 0.001$.

cotton swabs and two rooms using polyester swabs by rubbing nine swabs simultaneously across the surface of a 1 sq ft tile for 30 s or one entire door handle, respectively. Fecal samples included human, mouse and cat samples. Human feces were collected from two individuals using commode collectors (commode specimen collection system, Thermo Fisher Scientific, MA, USA). Mouse feces were collected from two individuals and stored in 1.5-ml microcentrifuge tubes. Cat feces were collected from two individuals and stored in plastic zip-top bags. Human urine samples included samples from female and male individuals. Urine was collected from three female and three male individuals and stored in commode collectors or 50-ml centrifuge tubes. Soil samples included tree rhizosphere and bare soil. For each type, soil was collected from two adjacent sites down to a depth of 20 cm using a sterile trowel and stored in plastic zip-top bags. Water samples included fresh- and seawater collected from two sites at the San Diego River and two sites at the Scripps Institution of Oceanography, respectively. Water was collected and stored in 50-ml centrifuge tubes. Fermented food samples included yogurt and sauerkraut samples. Two varieties of one brand of each food were purchased commercially and stored in 50-ml centrifuge tubes. Tissue samples included jejunum tissue from eight mice. Approximately 3.8 cm of the middle small intestine was removed, and any fecal matter inside was squeezed out lengthwise. Each tissue section was added to a 2-ml microcentrifuge tube containing 1 ml sterile $1\times$ phosphate-buffered saline and approximately 40 mg sterile 1-mm silicone beads and homogenized at 6000 rpm for 1 min with a MagNA Lyser (Roche Diagnostics, CA, USA). The liquid homogenate from three intestinal sections from cohoused mice was pooled to create a single sample (one sample per cage). All samples were stored at -80°C within 3 h of collection and frozen for a maximum of 24 h before extraction. To compare LOD – defined as the number of cells required to detect a microbe in the sequence data – the authors included serial dilutions of cultures of *Bacillus subtilis* (Firmicutes) and *Paracoccus denitrificans* (Alphaproteobacteria) [20]. Input cell densities ranged from 2.0 to $9.6\text{E}7$ cells for *B. subtilis* and 0.0 to $3.1\text{E}7$ cells for *P. denitrificans*. To compare well-to-well contamination [23], the authors included plasmid-borne, synthetic 16S rRNA gene spike-ins (i.e., 4 ng of unique spike-in to one well of each column in the plate) [28] and at least five extraction blanks per plate.

DNA and RNA extraction

The authors compared two extraction protocols that use a 96-sample magnetic bead cleanup format: the MagAttract PowerSoil DNA isolation kit (category number 27000-4-KF; Qiagen, CA, USA) and the MagMAX microbiome ultra nucleic acid isolation kit (category number A42357; Applied Biosystems, CA, USA). The authors considered that the PowerSoil kit protocol includes heating the lysis solution to 60°C when mixing with samples as well as a subsequent 20-min bead-beating step, whereas the MagMAX kit uses no heating and only a 2-min bead-beating step. Additional heating and extended bead-beating may alter the extent of cellular lysis and degradation of extracellular nucleic acids and, subsequently, microbial community composition. The authors therefore included a third protocol, a

Table 2. Results from a forward, stepwise model selection of factors influencing microbial community beta-diversity.

Data type	Distance metric	Factor	Adjusted R ²	df	AIC	F	p-value
16S	Unweighted UniFrac	Sample type	0.87	24	-556.59	172.97	0.0002
		Host identity	0.01	30	-583.89	2.85	0.0002
		Extraction protocol	0.001	2	-588.47	3.92	0.004
	Weighted UniFrac	Sample type	0.76	24	-165.42	79.55	0.0002
		Host identity	0.06	30	-320.67	7.83	0.0002
		Extraction protocol	0.001	2	-323.72	3.21	0.02
	Jaccard	Sample type	0.89	24	-651.49	206.18	0.0002
		Host identity	0.02	30	-756.85	5.76	0.0002
		Extraction protocol	0.001	2	-762.48	4.40	0.0008
	RPCA	Sample type	0.86	24	-495.50	154.16	0.0002
		Host identity	0.03	30	-619.04	6.49	0.0002
		Extraction protocol	0.001	2	-625.14	4.61	0.0002
Metagenomics	Unweighted UniFrac	Sample type	0.93	26	-958.24	317.60	0.0002
		Host identity	0.01	31	-1062.60	5.57	0.0002
		Extraction protocol	0.001	2	-1067.53	4.08	0.0006
	Weighted UniFrac	Sample type	0.87	26	-602.92	173.32	0.0002
		Host identity	0.02	31	-676.11	4.42	0.0002
		Extraction protocol	0.003	2	-693.97	10.09	0.0002
	Jaccard	Sample type	0.94	26	-1084.87	391.42	0.0002
		Host identity	0.01	31	-1217.42	6.67	0.0002
	RPCA	Sample type	0.85	26	-496.04	143.29	0.0002
		Host identity	0.03	31	-620.86	6.36	0.0002
		Extraction protocol	0.005	2	-645.41	13.24	0.0002

Values are based on permutation tests of variation explained by redundancy analysis, done separately for four unique metrics for both 16S and metagenomics data. The full model included bead-beating time (i.e., 2 vs 20 min), sample biomass (i.e., high vs low biomass), sample type, host subject identity and extraction protocol (i.e., MagMAX 2-min, MagMAX 20-min, PowerSoil) as model variables. The 16S data were rarefied, as noted for Figure 3. Metagenomics data were rarefied to 17,000 host- and quality-filtered reads per sample or had samples with fewer than 17,000 reads excluded when using RPCA distances (n = 647 samples). Rarefaction depths were selected to maintain at least 75% samples from both high- and low-biomass datasets.

AIC: Akaike information criterion; df: degrees of freedom; RPCA: Robust principal component analysis.

variant of the MagMAX protocol, including 60°C incubation and 20-min bead-beating steps, and refer to the three protocols as PowerSoil, MagMAX 20-min and MagMAX 2-min.

For extraction, aliquots of each sample were transferred to unique wells of a 96-well extraction plate. For samples collected with swabs, the entire swab head was broken off into the lysis plate. For liquid samples, the authors transferred 200 µl. For bulk samples, the authors used cotton swabs to collect approximately 100 mg of homogenized material and broke the entire swab head off into the lysis plate. Extractions were performed following the manufacturer's protocol, except for the modifications made to the previously described MagMAX 20-min protocol. Lysis was performed with a TissueLyser II (Qiagen). Bead clean-ups were performed with the KingFisher flex purification system (Thermo Fisher Scientific). Extracted nucleic acids were stored at -80°C prior to quantification of RNA yield, fragment length distribution and integrity as well as quantification of DNA yield and downstream sequencing.

16S rRNA gene and shotgun metagenomics sequencing

The authors prepared DNA for 16S rRNA gene and shallow shotgun metagenomics sequencing as described previously [10,29–31]. For 16S data, raw sequence files were demultiplexed using Qiita [32], and suboperational taxonomic units were generated using Deblur [33]. For shallow shotgun metagenomics data, raw sequence files were demultiplexed using BaseSpace (Illumina, CA, USA), quality-filtered using Atropos [34] and human read-depleted by alignment to human reference genome GRCh38 using bowtie2 [35]. Filtered reads were aligned to the Web of Life database [36] using Shogun [31] with default parameters and using bowtie2 as the aligner, followed by read classification with the Web of Life Toolkit App [36,37]. Raw sequence data were deposited at the European Nucleotide Archive (accession number ERP124610), and raw and processed data are available at Qiita (study identifier 12201). Processing and analysis code is available on GitHub (https://github.com/justinshaffer/Extraction_test_MagMAX).

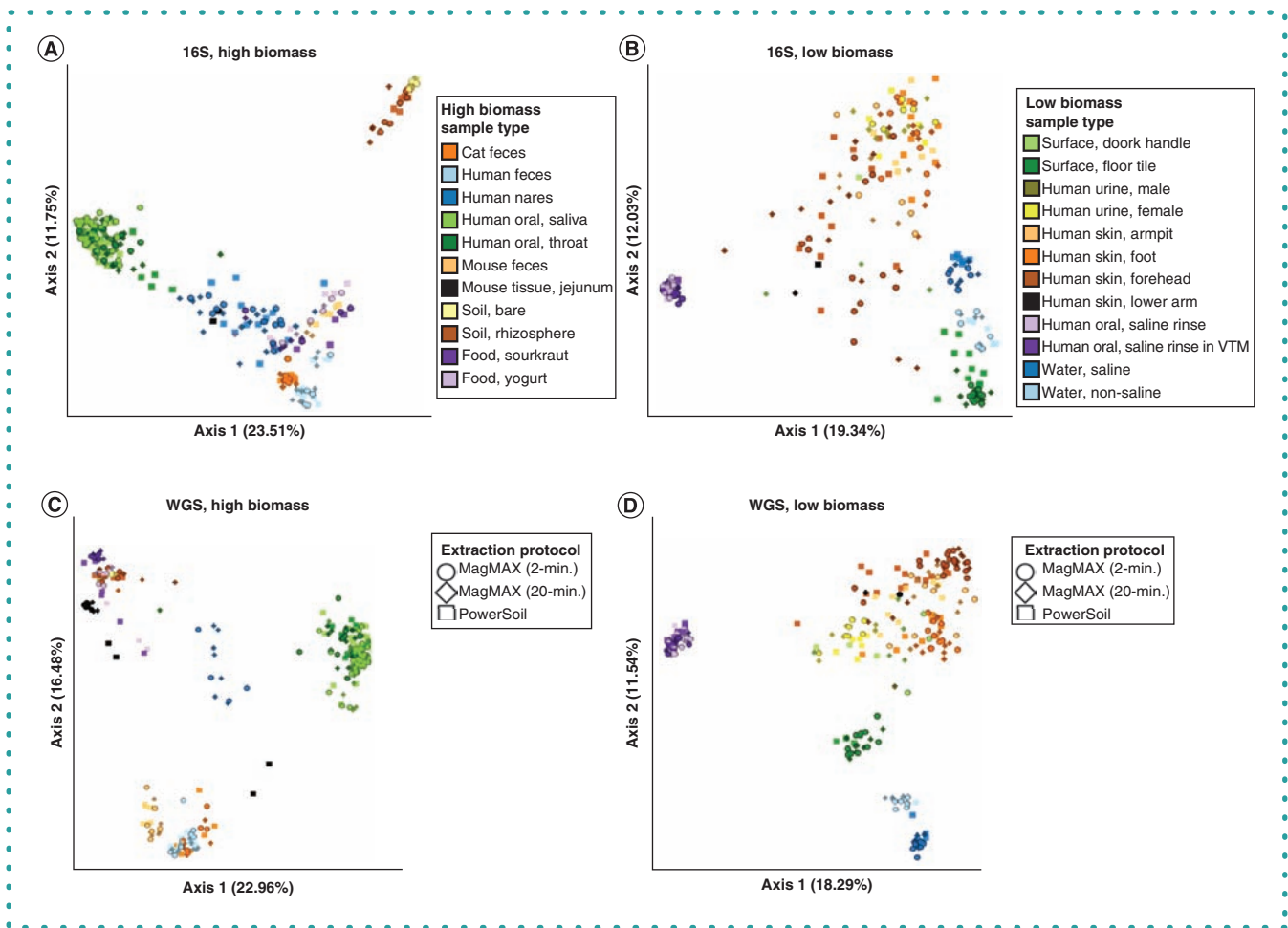


Figure 3. Beta-diversity among extraction protocols and sample types. Principal coordinates analysis (PCoA) plots showing unweighted UniFrac distances based on 16S data for (A) high biomass samples and (B) low biomass samples, and shotgun metagenomics data for (C) high biomass samples and (D) low biomass samples. Colors indicate sample types and shapes indicate extraction protocols. Mock community and control blanks were excluded for clarity. 16S data were rarefied to 5,000 quality-filtered reads per sample for both high- and low-biomass samples ($n = 611$ samples). Metagenomics data were rarefied to 35,000 host- and quality-filtered reads per high-biomass sample ($n = 287$ samples), and to 20,000 reads per low-biomass sample ($n = 242$ samples). When using RPCA distances rather than using rarefied data, we excluded samples with fewer reads than the rarefaction depth for that dataset. Rarefaction depths were selected to maintain at least 75% samples from both high- and low-biomass datasets.

Results & discussion

The authors found DNA yield to be similar across the three extraction protocols and note that when considering all sample types ($n = 615$ samples), the extraction efficiency of the PowerSoil protocol was more similar to that of the MagMAX 20-min protocol compared with MagMAX 2-min protocol (paired-sample Wilcoxon signed-rank test: PowerSoil vs MagMAX 20-min $W = 10,540$; $p = 0.6$ and PowerSoil vs MagMAX 2-min $W = 81,170$; $p = 0.01$) (Supplementary Figure 1). The authors observed a similar pattern for the number of quality-filtered 16S reads (PowerSoil vs MagMAX 20-min $W = 11,482$; $p = 0.1$ and PowerSoil vs MagMAX 2-min $W = 4651$; $p = 2.74E-11$). However, for quality- and human-filtered shotgun metagenomics reads, both MagMAX protocols varied from the PowerSoil protocol (PowerSoil vs MagMAX 20-min $W = 15,873$; $p = 1.41E-11$ and PowerSoil vs MagMAX 2-min $W = 17,148$; $p = 2.24E-15$) (Figure 1 & Supplementary Figure 2).

From a technical perspective, the authors' comparison of the LOD of each protocol indicates that the MagMAX 2-min protocol requires ten times the number of cells required by PowerSoil for accurate detection in mixed bacterial cultures (Table 1). This is compared with the 10,000 times required by the MagMAX 20-min protocol (Table 1). This pattern is mirrored when considering sample retention following filtering based on LOD thresholds, for which the MagMAX 2-min is better with high-biomass samples and the MagMAX 20-min with low-biomass samples. However, the authors observed an increase in well-to-well contamination in the MagMAX 20-min protocol compared with the MagMAX 2-min protocol (Figure 2). As all other parameters were consistent between the two MagMAX protocols, this indicates that mimicking lysis parameters from the PowerSoil protocol in the MagMAX protocol can have undesirable consequences.

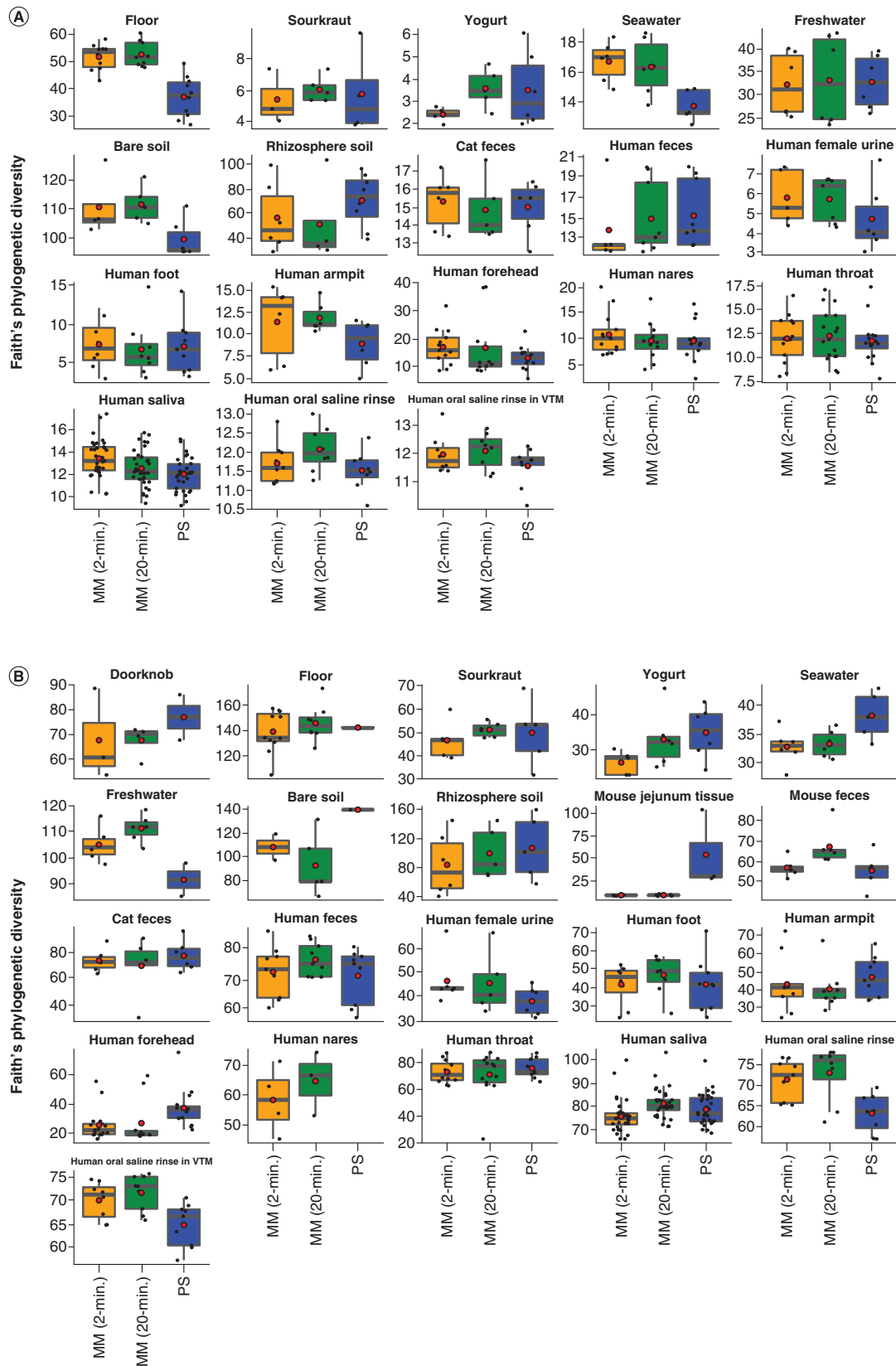


Figure 4. Alpha-diversity across extraction protocols and sample types. Faith's Phylogenetic Diversity among the three extraction protocols based on (A) 16S and (B) metagenomics data. Red circles indicate means. Data were rarefied as noted for Figure 3. MM: MagMAX; PS: PowerSoil.

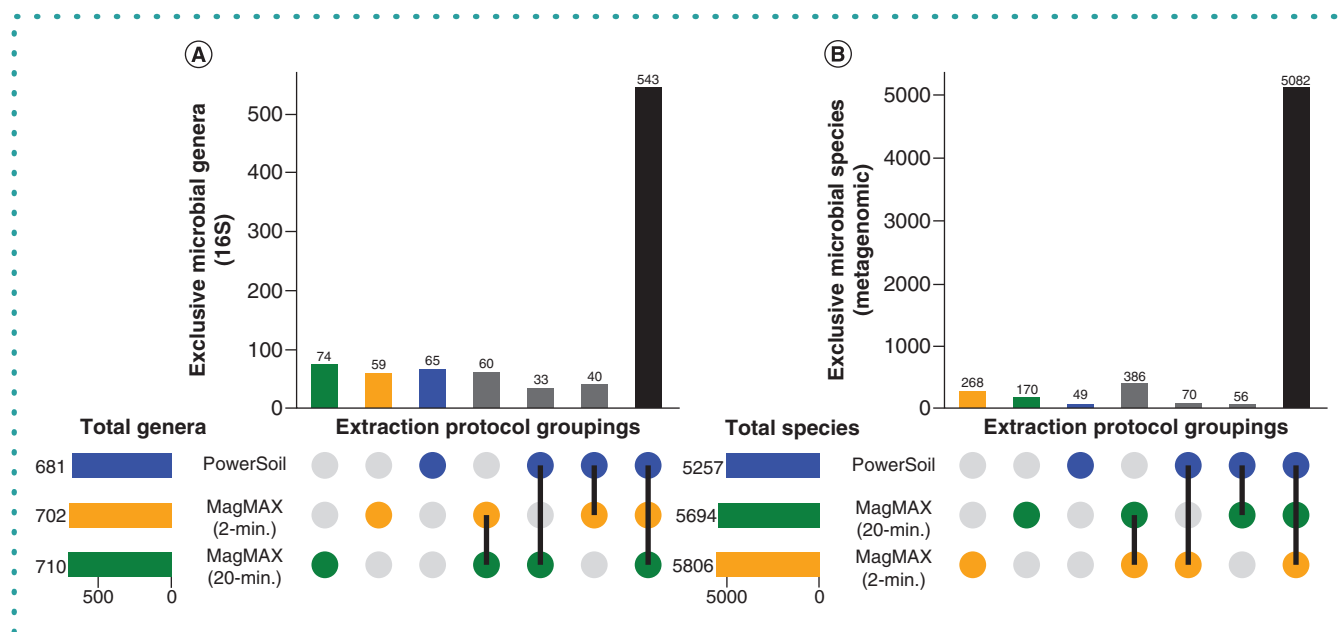


Figure 5. Taxonomic bias among extraction protocols. Upset plots showing (A) genera for 16S data and (B) species for metagenomics data, highlighting taxa shared among extraction protocols. Data were rarefied as noted for Figure 3.

The extended bead-beating time may lead to lysate leaking into the thin ridges of the 96-well plate, which is covered by a plastic film. From this perspective, the authors favor the MagMAX 2-min protocol.

With respect to microbial community composition, the authors found bias introduced by extraction protocol to be small compared with variation among sample types or replicates of the same sample (i.e., one to two orders of magnitude weaker in explaining beta-diversity) (Tables 1 & 2 & Supplementary Figures 3 & 4). The authors also found strong correlations in microbial community beta-diversity among samples between any two extraction protocols; however, relationships with the PowerSoil protocol were slightly stronger for MagMAX 2-min compared with MagMAX 20-min (Supplementary Table 1). The authors used principal coordinates analysis of unweighted UniFrac distances to visualize these trends and confirmed that samples clustered strongly by type and host subject and not by extraction protocol for both 16S and metagenomics data (Figure 3 & Supplementary Figures 5 & 6). Estimates of alpha-diversity were more comparable to those from PowerSoil for the MagMAX 2-min protocol (paired-sample Wilcoxon signed-rank test: PowerSoil vs MagMAX 2-min $W = 5916$; $p = 0.0001$ and PowerSoil vs MagMAX 20-min $W = 7058$; $p = 1.53E-06$) (Figure 4 & Supplementary Figure 7). Finally, the majority of genera (16S) and species (metagenomics) were shared across all three extraction protocols; however, for both datasets, the MagMAX 2-min protocol shared a greater number of exclusive taxa with the PowerSoil protocol than the MagMAX 20-min protocol did (Figure 5).

Together, these results highlight that, despite variation in DNA yield, sequence read counts and LOD of microbial cells among extraction protocols, differences in microbial taxonomic and community composition resulting from the different methods were minor for both 16S and metagenomics microbial sequence data. However, between the two MagMAX protocols, the authors note that for beta-diversity, alpha-diversity and taxonomic composition, the MagMAX 2-min protocol generated results more comparable to the PowerSoil protocol.

Importantly, whereas RNA yield was comparable between the two MagMAX protocols (Figure 6A), the authors observed a higher quality of extracted RNA using the MagMAX 2-min versus MagMAX 20-min protocol (Figure 6B & C). In addition to reduced well-to-well contamination from a shorter bead-beating time during lysis for the MagMAX 2-min versus MagMAX 20-min protocol, the lack of incubation of the lysis buffer resulted in relatively high-quality RNA produced with the former compared with the latter (Figure 6).

Conclusion

We conclude that the MagMAX 2-min extraction protocol is comparable to our established PowerSoil protocol with respect to characterizing microbial community composition and therefore should allow for comparisons such as meta-analysis across 16S and metagenomics data produced using both protocols and downstream methods similar to those used here. In addition to extracting both DNA and RNA, the more rapid processing time (i.e., approximately 2 h faster than PowerSoil per 96 samples), use of fewer consumables (i.e., approximately 70% of plastics) and lower cost (i.e., \$5.56 vs \$5.65 per sample) highlight the MagMAX 2-min protocol as a comparable and efficient alternative to the PowerSoil protocol that also allows for downstream applications using RNA.

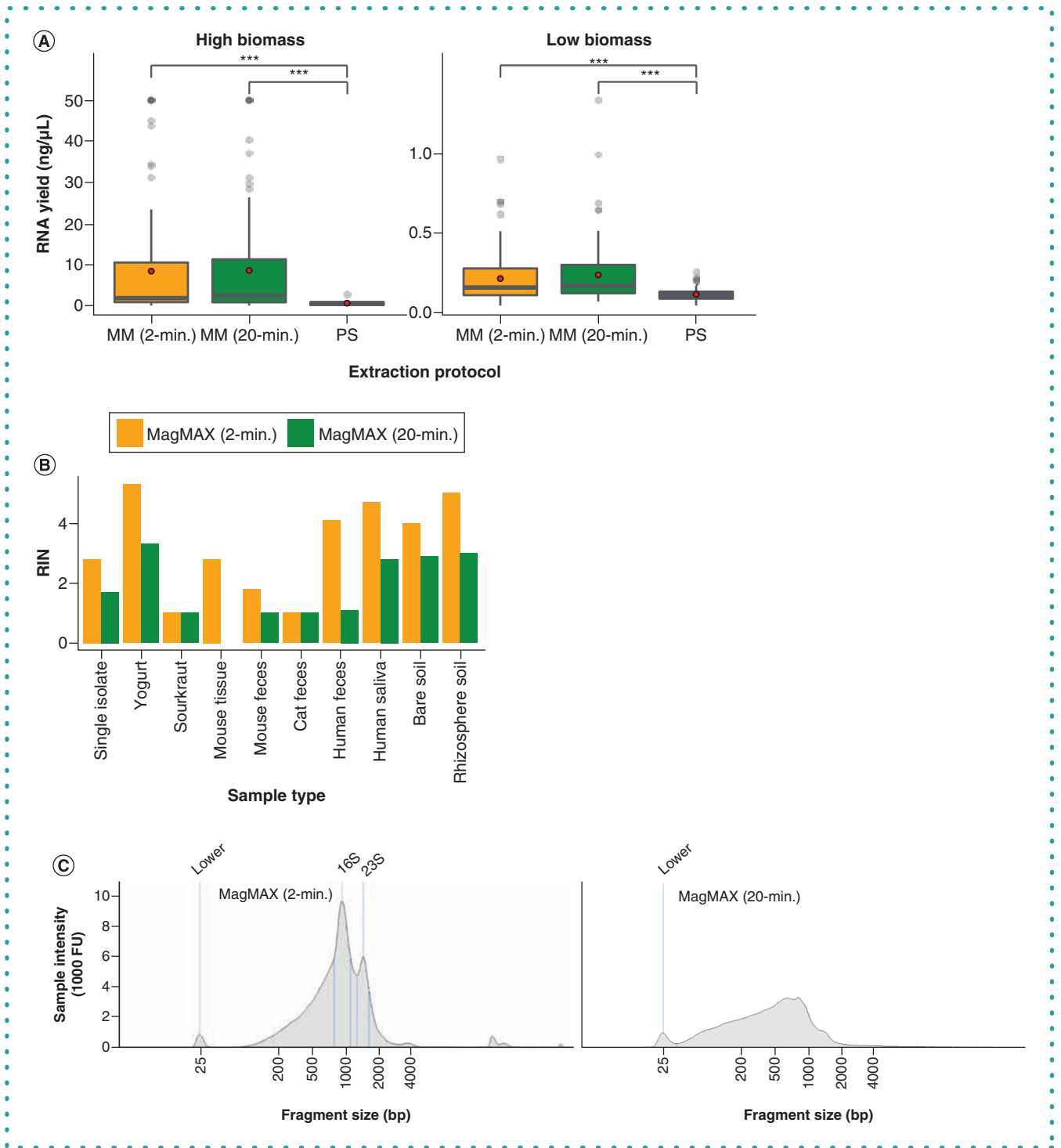


Figure 6. RNA output across extraction protocols. (A) RNA yield quantified using the Qubit RNA assay. Red circles indicate means. Asterisks indicate significant differences between pairs of extraction protocols as determined by paired-sample Wilcoxon signed-rank tests; $***p < 2.2E-16$. Values at 50 ng/ μ L are at the upper limit of detection for the Qubit assay, and may underestimate actual yields for those samples. **(B)** RNA Integrity Number (RIN) across a subset of samples for the MagMAX extraction protocols, estimated using the TapeStation high-sensitivity (HS) RNA assay. PowerSoil extracts were excluded from the assay due to poor RNA yield, however we note that this may be to our exclusion of the RNase step available in that protocol. **(C)** RNA fragment length distribution estimated using the TapeStation HS RNA assay for one human fecal sample. The distribution for the MagMAX (2-min) is on the left and that for the MagMAX (20-min) on the right. The positive control marker at 25-bp is annotated. Peaks corresponding to expected lengths for 16S and 23S rRNA are annotated for the 2-min. protocol and are missing from output from the 20-min. one. MM: MagMAX; PS: PowerSoil.

Future perspective

Future optimization of molecular methods for microbial community analyses should focus on increasing representation of all microbes in a sample as well as diverse sample types, including those used here. Achieving these goals will allow for more widely adopted use of the same methods. As no single study can be completely comprehensive, making advances that allow us to better compare across studies, particularly past studies, is an important step [38]. Alongside the development of computational methods that bioinformatically reduce experimental variation, continuing to explore new molecular methods for capturing important ecological interactions will support our growing understanding of microbial communities.

Executive summary

- Established protocols were compared for DNA extraction with two alternative protocols that also extract RNA.
- The authors included a diverse panel of sample types, ranging from host-associated to environmental.
- Controls were included for detecting well-to-well contamination and LOD of microbial cells.
- The authors observed sample type-specific differences in DNA extraction efficiency among three extraction protocols.
- Both new protocols were similar with respect to RNA extraction efficiency but varied in RNA quality.
- Sample type and host identity were stronger drivers of microbial community beta-diversity compared with the extraction protocol used.
- A protocol was identified that generates both DNA and RNA and produces data that are highly similar to their established protocol with respect to microbial community alpha-diversity, beta-diversity and taxonomic composition.
- The similarity between the optimal protocol and the authors' existing protocol will allow for meta-analyses across both with negligible technical bias.

Supplementary data

To view the supplementary data that accompany this paper please visit the journal website at: www.future-science.com/doi/suppl/10.2144/btn-2020-0153

Author contributions

JP Shaffer, C Marotz, P Belda-Ferre, RA Salido, CS Carpenter, LS Zaramela, JJ Minich, G Humphrey, AD Swafford, S Miller-Montgomery and R Knight designed the study; JP Shaffer, C Marotz, P Belda-Ferre, RA Salido, CS Carpenter, L Zaramela, M Bryant and G Humphrey provided samples; JP Shaffer, C Marotz, CS Carpenter and S Fraraccio performed extractions; RA Salido, M Bryant, K Sanders and G Humphrey performed quality control and sequencing; JP Shaffer, C Marotz, P Belda-Ferre, C Martino, S Wandro, M Estaki and RA Salido performed data analyses; and JP Shaffer wrote the manuscript, with contributions from all authors.

Acknowledgments

The authors thank K Dao, R Moranchel, C Nguyen, C Morris and R Simpson for providing samples and J DeReus for assistance with data processing.

Financial & competing interests disclosure

JP Shaffer was supported by NIH San Diego Institutional Research and Academic Career Development Award (5K12GM068524-17) and the United States Department of Agriculture - National Institute of Food and Agriculture (USDA-NIFA) (2019-67013-29137). C Martino was supported by NIH (1RF1-AG058942-01) and Semiconductor Research Corporation and Defense Advanced Research Projects Agency (SRC/DARPA) (GI18518). P Belda-Ferre was supported by National Science Foundation - Center for Aerosol Impacts on Chemistry of the Environment and Crohn's & Colitis Foundation Award (CCFA) (675191). G Ackermann was supported by NIH (R01HL140976, R01DK102932, R01HL134887) and Department of Defense (W81XWH-17-1-0589). G Humphrey was supported by NIH (U19AG063744, U01 AI124316), Office of Naval Research (ONR) (N00014-15-1-2809) and the Emerald Foundation (3022). R Knight was supported by NIH (1RF1-AG058942-01, 1DP1AT010885, R01HL140976, R01DK102932, R01HL134887), USDA-NIFA (2019-67013-29137), SRC/DARPA (GI18518), CCFA (675191), ONR (N00014-15-1-2809) and the Emerald Foundation (3022). The authors have no other relevant affiliations or financial involvement with any organization or entity with a financial interest in or financial conflict with the subject matter or materials discussed in the manuscript apart from those disclosed.

No writing assistance was utilized in the production of this manuscript.

Ethical conduct of research

The authors state that they have obtained appropriate institutional review board approval; the human subject work conducted here has been approved through University of California, San Diego IRB#150275. In addition, informed consent has been obtained from the participants involved.

Open access

This work is licensed under the Attribution-NonCommercial-NoDerivatives 4.0 Unported License. To view a copy of this license, visit <http://creativecommons.org/licenses/by-nc-nd/4.0/>

References

Papers of special note have been highlighted as: • of interest; •• of considerable interest

1. Kelly CR, Ihunnah C, Fischer M *et al.* Fecal microbiota transplant for treatment of *Clostridium difficile* infection in immunocompromised patients. *Am. J. Gastroenterol.* 109(7), 1065–1071 (2014).
2. Bokulich NA, Chung J, Battaglia T *et al.* Antibiotics, birth mode, and diet shape microbiome maturation during early life. *Sci. Transl. Med.* 8(343), 343ra82 (2016).
3. Panke-Buisse K, Poole AC, Goodrich JK, Ley RE, Kao-Kniffin J. Selection on soil microbiomes reveals reproducible impacts on plant function. *ISME J.* 9, 980–989 (2015).
4. Bell TH, Stefani FP, Abram K *et al.* A diverse soil microbiome degrades more crude oil than specialized bacterial assemblages obtained in culture. *Appl. Environ. Microbiol.* 82(18), 5530–5541 (2016).
5. Dominguez-Bello MG, Godoy-Vitorino F, Knight R, Blaser M.J. Role of the microbiome in human development. *Gut* 68, 1108–1114 (2019).
6. Poore GD, Kopylova E, Zhu Q *et al.* Microbiome analysis of blood and tissues suggest cancer diagnostic approach. *Nature* 579, 567–574 (2020).
7. Taylor BC, Lejzerowicz F, Poirel M *et al.* Consumption of fermented foods is associated with systematic differences in gut microbiome and metabolome. *mSystems* 5(2), e00901-19 (2020).
8. Knight R, Vrbanac A, Taylor BC *et al.* Best practices for analysing microbiomes. *Nat. Rev. Microbiol.* 16, 410–422 (2018).
9. Bolyen E, Rideout JR, Dillon MR *et al.* Reproducible, interactive, scalable, and extensible microbiome data science using QIIME2. *Nat. Biotechnol.* 37, 852–857 (2019).
10. Sanders JG, Nurk S, Salido RA *et al.* Optimizing sequencing protocols for leaderboard metagenomics by combining long and short reads. *Genome Biol.* 20(1), 226 (2019).
11. Song SJ, Amir A, Metcalf JL *et al.* Preservation methods differ in fecal microbiome stability, affecting suitability for field studies. *mSystems* 1(3), e00021-16 (2016).
- **Highlights the importance of considering how samples are maintained prior to processing for analysis of microbial communities.**
12. Parada AE, Needham DM, Fuhrman JA. Every base matters: assessing small subunit rRNA primers for marine microbiomes with mock communities, time series and global field samples. *Environ. Microbiol.* 18(5), 1403–1414 (2016).
13. Bjerre RD, Hugerth LW, Boulund F, Seifert FM, Johansen JD, Engstrand L. Effects of sampling strategy and DNA extraction on human skin microbiome investigations. *Sci. Rep.* 9(1), 17287 (2019).
- **Important for understanding the influence of technical factors on analysis of microbial communities.**
14. WHO. Coronavirus disease (COVID-19) weekly situation report, October 18, 2020. www.who.int/docs/default-source/coronaviruse/situation-reports/20200928-weekly-epi-update.pdf?sfvrsn=9e354665_6
15. Domingues CPF, Rebelo JS, Dionisio F, Botelho A, Nogueira T. The social distancing imposed to contain COVID-19 can affect our microbiome: a double-edged sword in human health. *mSphere* 5(5), e00716-20 (2020).
16. Hughes S, Troise O, Donaldson H, Mughal N, Moore LSP. Bacterial and fungal coinfection among hospitalized patients with COVID-19: a retrospective cohort study in a UK secondary-care setting. *Clin. Microbiol. Infect.* 26, 1395–1399 (2020).
- **Highlights the importance of understanding interactions of SARS coronavirus 2 (SARS-CoV-2) with other illnesses caused by bacteria and fungi.**
17. Zuo T, Zhang F, Lui G *et al.* Alterations in gut microbiota of patients with COVID-19 during time of hospitalization. *Gastroenterol.* 159, 944–955 (2020).
18. Marotz C, Amir A, Humphrey G, Gaffney J, Gogul G, Knight R. DNA extraction for streamlined metagenomics of diverse environmental samples. *BioTechniques* 62(6), 290–293 (2017).
- **Important for understanding differences in DNA extraction methods, particularly different bead clean-up methods, for downstream analysis of microbial communities.**
19. Khailany RA, Safdar M, Ozaslan M. Genomic characterization of a novel SARS-CoV-2. *Gene Rep.* 19, 100682 (2020).
20. Minich JJ, Zhu Q, Janssen S *et al.* KatharoSeq enables high-throughput microbiome analysis from low-biomass samples. *mSystems* 3(3), e00218-17 (2018).
- **Important for understanding differences in DNA extraction methods for regular or high- versus low-biomass sample types for analysis of microbial communities.**
21. Salter SJ, Cox MJ, Turek EM *et al.* Reagent and laboratory contamination can critically impact sequence-based microbiome analysis. *BMC Biol.* 12, 87 (2014).
22. Eisenhofer R, Minich JJ, Marotz C, Cooper A, Knight R, Weyrich LS. Contamination in low microbial biomass microbiome studies: issues and recommendations. *Trends Microbiol.* 27(2), 105–117 (2019).
23. Minich JJ, Sanders JG, Amir A, Humphrey G, Gilbert JA, Knight R. Quantifying and understanding well-to-well contamination in microbiome research. *mSystems* 4(4), e00186-19 (2019).
24. Sehulster LM, Chinn RYW, Arduino MJ *et al.* Guidelines for environmental infection control in health-care facilities. In: *Recommendations from CDC and the Healthcare Infection Control Practices Advisory Committee (HICPAC)*. American Society for Healthcare Engineering/American Hospital Association, IL, USA (2004).
25. CDC. Specimen collection guidelines. 1–8 (2020). www.cdc.gov/urdo/downloads/SpecCollectionGuidelines.pdf
26. Thompson LR, Sanders JG, McDonald D *et al.* A communal catalogue reveals Earth's multiscale microbial diversity. *Nature* 551, 457–463 (2017).
27. CDC. Preparation of viral transport medium. SOP#: DSR-052-02. 1–8 (2020). www.cdc.gov/coronavirus/2019-ncov/downloads/Viral-Transport-Medium.pdf
28. Tourlousse DM, Yoshiike S, Ohashi A, Matsukura S, Noda N, Sekiguchi Y. Synthetic spike-in standards for high-throughput 16S rRNA gene amplicon sequencing. *Nucleic Acids Res.* 45(4), e23 (2017).
29. Caporaso JG, Lauber CL, Walters WA *et al.* Ultra-high-throughput microbial community analysis on the Illumina HiSeq and MiSeq platforms. *ISME J.* 6, 1621–1624 (2012).
30. Minich JJ, Humphrey G, Benitez RAS *et al.* High-throughput miniaturized 16S rRNA amplicon library preparation reduces costs while preserving microbiome integrity. *mSystems* 3(6), e00166-18 (2018).
31. Hillmann B, Al-Ghalith GA, Shields-Cutler RR *et al.* Evaluating the information content of shallow shotgun metagenomics. *mSystems* 3(6), e00069-18 (2018).
32. Gonzalez A, Navas-Molina JA, Kosciolk T *et al.* Qiita: rapid, web-enabled microbiome meta-analysis. *Nat. Methods* 15, 796–798 (2018).
33. Amir A, McDonald D, Navas-Molina JA *et al.* Deblur rapidly resolves single-nucleotide community sequence patterns. *mSystems* 2(2), e00191-16 (2017).
34. Didion JP, Martin M, Collins FS. Atropos: specific, sensitive, and speedy trimming of sequencing reads. *PeerJ* 5, e3720 (2017).
35. Langmead B, Salzberg SL. Fast gapped-read alignment with Bowtie 2. *Nat. Methods* 9(4), 357–359 (2012).
36. Zhu Q, Mai U, Pfeiffer W *et al.* Phylogenomics of 10,575 genomes reveals evolutionary proximity between domains Bacteria and Archaea. *Nat. Commun.* 10(1), 5477 (2019).
37. Zhu Q. Web of Life Toolkit App. <https://github.com/qiyunzhu/woltka>
38. Greathouse KL, Sinha R, Vogtmann E. DNA extraction for human microbiome studies: the issue of standardization. *Genome Biol.* 20(1), 212 (2019).

An engraved surface induces weak adherence and high proliferation of nonadherent cells and microorganisms during culture

Sunil Thomas*,¹ 

¹Lankenau Institute for Medical Research, Wynnewood, PA 19096, USA; *Author for correspondence: suntom2@gmail.com

BioTechniques 69: 113–125 (August 2020) 10.2144/btn-2020-0022

First draft submitted: 4 March 2020; Accepted for publication: 21 May 2020; Published online: 12 June 2020

ABSTRACT

When cells are cultured in a Petri dish, the adherent cells attach to the bottom of the dish; whereas, the nonadherent cells float in the culture medium. It was observed that nonadherent cells could be induced to adherent-like cells when cultured in an engraved plastic dish (biosimulator). The adherence of these cells to the engraved surface could be prevented with inhibitors specific for adhesion. It was also observed that culturing microorganisms of the environment in a biosimulator induced weak adhesion and high proliferation. Analysis of the microbiome using 16S rRNA profiling demonstrated that the biosimulator was more efficient in inducing proliferation of several phyla of microorganisms compared with culture by conventional techniques.

METHOD SUMMARY

Nonadherent cells could be induced to adherent-like cells when cultured in an engraved plastic dish (biosimulator). The adhesion induced proliferation of eukaryotic and prokaryotic cells.

KEYWORDS:

adherence • biosimulator • cell culture • diagnostics • engraving • environment • microbiome • microorganisms • nonadherent cells • Petri dish

Cell culture is routinely employed in laboratories for biomedical research and has multiple applications, including diagnosis, drug development, therapy and production of biological resources. The traditional process of culturing adherent cells in a Petri dish still serves as an important tool for cell culture applications [1]. During cell culture, the adherent cells attach to the bottom of a plastic Petri dish, whereas nonadherent cells float in the culture medium. There are no specialized dishes for transforming nonadherent cells to adherent cells; this is an impediment in several drug development studies, especially in those involving autoreactive T cells or cells involved in atherosclerosis.

The majority of microorganisms of the environment are nonculturable [2]. In addition, some microorganisms exist in a viable but nonculturable state and are difficult to culture in laboratory conditions. Such cells are characterized by a lack of culturability using conventional culture techniques that impairs their detection by routine analytical techniques. This leads to an underestimation of total viable cells in environmental or clinical samples, and thereby poses a risk to public health [3]. Hence, there is a need to develop a strategy to increase the proliferation of such microorganisms.

In this paper, it is demonstrated that nonadherent cells exhibit adherence when cultured in an engraved polystyrene Petri dish. Though the cells cultured were from the same clone, when cultured on an engraved dish, they exhibited polarity. It was also demonstrated that specific inhibitors could be used to prevent adhesion of nonadherent cells on an engraved surface. Further, we demonstrate that the biosimulator enhanced the proliferation of microorganisms. The phenomenon of cell adhesion on an engraved dish has wide applications in cell biology and microbiology.

Materials & methods

Development of a biosimulator to induce adhesion & proliferation of cells

For culturing cells, nonpyrogenic, noncytotoxic and polystyrene BioLite cell culture dishes (Thermo Scientific, NJ, USA) were used. To induce adhesion of cells, the plastic surface was engraved with parallel lines using a sterile sharp blade under aseptic conditions. The engravings had a width of 30–50 μm and depth of 5 μm .

Cell culture in the biosimulator

The nonadherent hybridoma cell lines 4B7, 10D9, 1A10, 99D, Sp2/0, B56T (1×10^6 cells/dish) were cultured in 10 ml Dulbecco's modified Eagle medium, and incubated at 37°C, 5% CO₂. The cells were monitored daily. All the experiments were repeated at least three times.

For cell proliferation assays, hybridoma cells were grown in a conventional dish or a biosimulator. Cells were collected every other day, depending on the proliferation. The absorption of cells was measured at 600 nm using a spectrophotometer; a hemocytometer was used for cell count.

For inhibition of cell adhesion, 0.1% salicylic acid (Fisher Scientific, NJ, USA) and 0.01% pectasol (gift of ecoNugenics, CA, USA) were added to the culture medium during cell culture.

Proliferation & analyses of microorganisms in a biosimulator

Samples from soil, spring water, air (office) and host oral microbiome were cultured in a biosimulator in Luria-Bertani medium for 48 h. After 48 h, the media were pelleted in a centrifuge at 5000×g and the samples subjected to 16S rRNA sequencing (Arizona State University Microbiome Core) for taxonomic identification. Microbial DNA was extracted from samples using the DNeasy PowerSoil Kit (Qiagen, Germany) following the manufacturer's directions.

Microbiome library preparation methodology

Bacterial community analysis was performed via next generation sequencing on the Illumina MiSeq platform. Amplicon sequencing of the V4 region of the 16S rRNA gene was performed with the barcoded primer set 515f/806r designed by Caporaso *et al.* [4] and following the protocol by the Earth Microbiome Project (<http://www.earthmicrobiome.org/emp-standard-protocols/>) for library preparation. PCR amplifications for each sample were done in triplicate, then pooled and quantified using the Quant-iT™ PicoGreen® dsDNA Assay Kit (Invitrogen, CA, USA). A no-template control sample was included during library preparation as a control for extraneous nucleic acid contamination. About 240 ng of DNA per sample were pooled and then cleaned using the QIAquick PCR purification kit (Qiagen). The pool was quantified using the Illumina library Quantification Kit ABI Prism® (Kapa Biosystems, MA, USA), then diluted to a final concentration of 4 nM, denatured, and diluted to a final concentration of 4 pM with 15% of PhiX control library (Illumina, CA, USA). Finally, the DNA library was loaded in the MiSeq and run using the version 2 module, 2 × 250 paired end, following the directions of the manufacturer.

Analysis of sequencing results was performed by the University of North Carolina Microbiome Core. The sequencing output from the MiSeq platform was converted to FASTQ format and demultiplexed using Bcl2Fastq 2.18.0.12 (Illumina). The resulting paired-end reads were processed using QIIME 2 2018.11. Index and linker primer sequences were trimmed using the QIIME 2 invocation of cutadapt. The resulting paired-end reads were processed with DADA2 through QIIME 2, including merging paired ends, quality filtering, error correction and chimera detection.

Amplicon sequencing units from DADA2 were assigned taxonomic identifiers according to Green Genes release 13.08, the Human Oral Microbiome Database release 15.1 and Silva database release 132.

Alpha diversity with respect to Faith PD whole tree, Evenness (Shannon) index and observed species number metrics was estimated using QIIME 2 at a rarefaction depth of 5000 sequences per subsample. Beta diversity estimates were calculated within QIIME 2 using weighted and unweighted Unifrac distances as well as Bray–Curtis dissimilarity between samples at a subsampling depth of 5000. Results were summarized, visualized through principal coordinate analysis and significance was estimated as implemented in QIIME 2. Significance of differential abundance was estimated using AnCom as implemented in QIIME 2.

Statistics

Unpaired two-tailed Student *t*-tests were used to compare sets of data obtained from independent groups. Statistical significance was considered at the $p < 0.05$ level.

Results & discussion

An engraved surface could induce adhesion of nonadherent cells

Based on the observation that a cell culture plate with a compromised surface has high affinity for cells, parallel lines were engraved on a tissue culture Petri dish and used the dish for cell culture. The cells were nonadherent and were found floating on the first and second day of culture. After 3 days of culture, all the cell lines tested (4B7, 10D9, 1A10, 99D, Sp2/0, 99D) formed distinct patterns on the engraved plastic surface; pattern formation corresponded to the engraving. When the Petri dish was engraved with parallel lines, the nonadherent cells were seen on top of the engraved line, whereas on the lower half of the dish the nonadherent cells were below the engraved line (Figure 1). The orientation of the cells is shown in Figure 1C & D. The cells were closely packed on the engraved line. The alignment of nonadherent cells was found to be stable on the engraved line; minor disturbances to the plastic dish did not destroy the patterns exhibited. This failure to destroy the patterns demonstrated that the cells were adhered near the engraved surface. The experiment demonstrated that an engraved surface could induce nonadherent cells to become adherent cells.

In conventional cell culture, adherent cells grow to confluence, and must be dissociated from the dish using trypsin. In our experiment, the nonadherent cells (unlike the adherent cells) were not strongly adhered to the biosimulator. Liquid media were pipetted to disrupt

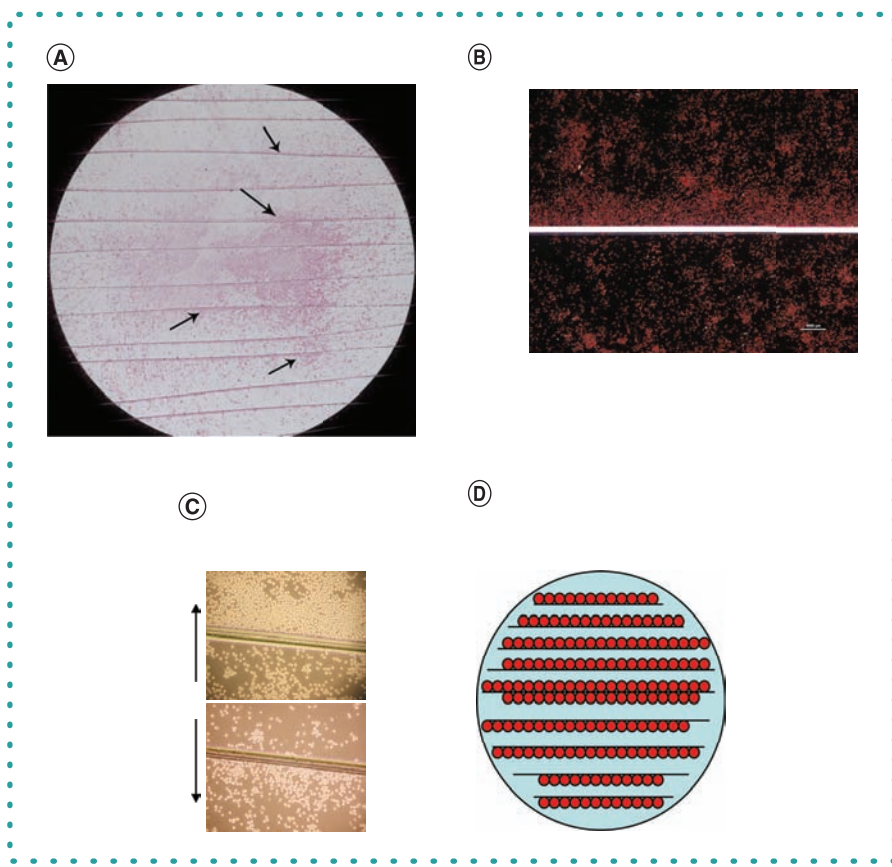


Figure 1. Engraved surface-induced adhesion of nonadherent cells. (A) Photomicrograph of nonadherent cells (4B7) exhibiting polarity on an engraved dish (biosimulator). (B) Ponceau S staining of cells cultured in a biosimulator. (C) The orientation of cells in a biosimulator. Cells are aligned on top of the engraving in the upper half of the biosimulator, whereas they are aligned below the engraving in the bottom half of the biosimulator. (D) Drawing of an engraved Petri dish showing the orientation of nonadherent cells. Experiments were repeated five times.

the cells from a distance of 1 cm. Seventy percent of the cells were removed when the media was pipetted at a speed of 5 ml per 10 s (repeated five times). The experiment demonstrated that the nonadherent cells are weakly adhered to the engraving of the biosimulator.

An engraved surface induced proliferation of nonadherent cells

We determined whether the engraved surface induced proliferation of nonadherent cells. B cell hybridoma cell lines 99D (Figure 2) and 4B7 (Figure 3) were cultured in an engraved biosimulator, using conventional Petri dishes as a control. We counted the cells and also determined the absorbance (optical density at 600 nm) at regular intervals. The biosimulator induced proliferation of the nonadherent cells, as determined by cell counting and absorbance measurements (Figures 2 & 3). Culture of nonadherent cells in a biosimulator led to a statistical increase in the number of cells compared with culturing in conventional Petri dishes. The study demonstrated that engraving patterns in a biosimulator could induce adhesion and proliferation of nonadherent cells.

Adhesion of nonadherent cells in a biosimulator could be inhibited by specific inhibitors

Salicylic acid is known to prevent cell–cell interaction and is used in animal models of diabetes [5], but its mechanism of action is not clearly known. When nonadherent cells (4B7) were treated with 0.1% salicylic acid, cell adhesion was inhibited (Figure 4). We also used the adhesion inhibitor pectasol (which prevents cancer metastasis) in our studies [6]. Treatment of nonadherent cells with 0.01% pectasol did not prevent cell proliferation; however, it prevented cells adhering to the plastic surface (Figure 4C). The nonadherent cells lost the orientation property; the cells were found floating in the medium and did not have any affinity for the engraved surface. These *in vitro* experiments demonstrate that the phenomenon of pattern formation could be used in drug discovery studies.

The engraved surface-induced proliferation of microorganisms

As the engraved surface in the biosimulator could induce cell proliferation, we were interested to determine whether it could also induce proliferation of microorganisms. One of the impediments in microbial studies or diagnosis is the nonculturable property of most of the microorganisms. Only a very limited number of microorganisms are culturable by conventional culture techniques; there is therefore a

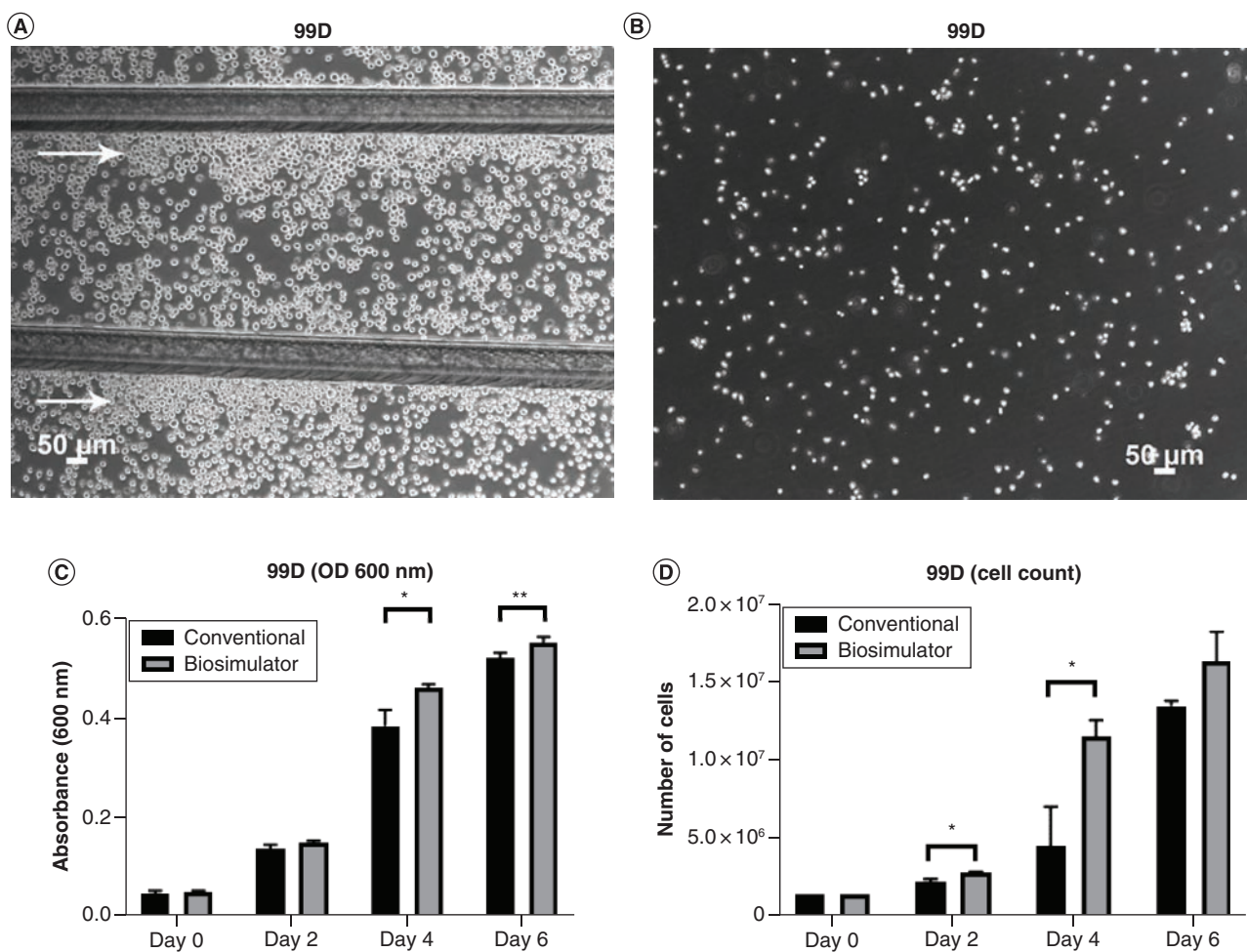


Figure 2. Engraved surface-induced proliferation of 99D nonadherent cells. The hybridoma cell 99D was induced to proliferate by the engraved surface. **(A)** Photomicrograph showing 99D cells adhering to the engraving of a biosimulator compared with **(B)** growth in a conventional dish. **(C)** Absorbance at 600 nm of 99D cells growing in a biosimulator or conventional dish. **(D)** Cell count of 99D cells growing in a biosimulator or conventional dish using a hemocytometer. Experiments were repeated five times. * $p < 0.05$, ** $p < 0.01$ as determined by *t*-test.

need to develop new strategies to induce proliferation of microorganisms. The microbiome is involved in health and diseases [7] and there is a need to determine dysbiotic microorganisms to facilitate diagnosis and treatment.

Samples were cultured from different environments – air, water, soil and host oral cavity – in the biosimulator. The microorganisms were found to adhere to the engravings of the biosimulator within 24 h (Figure 5). After 48 h, they proliferated and covered the entire biosimulator. Analysis of the soil microbiome by spectrometry demonstrated that the biosimulator induced more proliferation of the microorganisms compared with conventional techniques (Figure 5).

The biosimulator induced proliferation of a large number of Firmicutes in samples from air, soil, water and oral cavity compared with culture using conventional techniques (Figure 6). The phylum Firmicutes includes the class Clostridia and genus *Clostridium* and consists of a large group of anaerobic to aerotolerant spore-forming bacilli found in soil and in the gut flora of humans and animals. Clostridia include both gram-positive and gram-negative species, although the majority are gram-positive. Interestingly, many gram-positive species lose the Gram reaction, resulting in gram-negative cultures [8]. Some species of *Clostridium* can become aerotolerant on subculture; however, only a few (*C. carnis*, *C. histolyticum*, and *C. tertium*) can grow under aerobic conditions. The vast majority of human oral Clostridia comprises the families Lachnospiraceae, Peptostreptococcaceae and Veillonellaceae [9]. Microbial sequencing demonstrated that the biosimulator induced proliferation of bacterial phyla of air (Figure 7, Supplementary Table 1), water (Figure 8, Supplementary Table 2), soil (Figure 9, Supplementary Table 3) and oral samples (Figure 10, Supplementary Table 4).

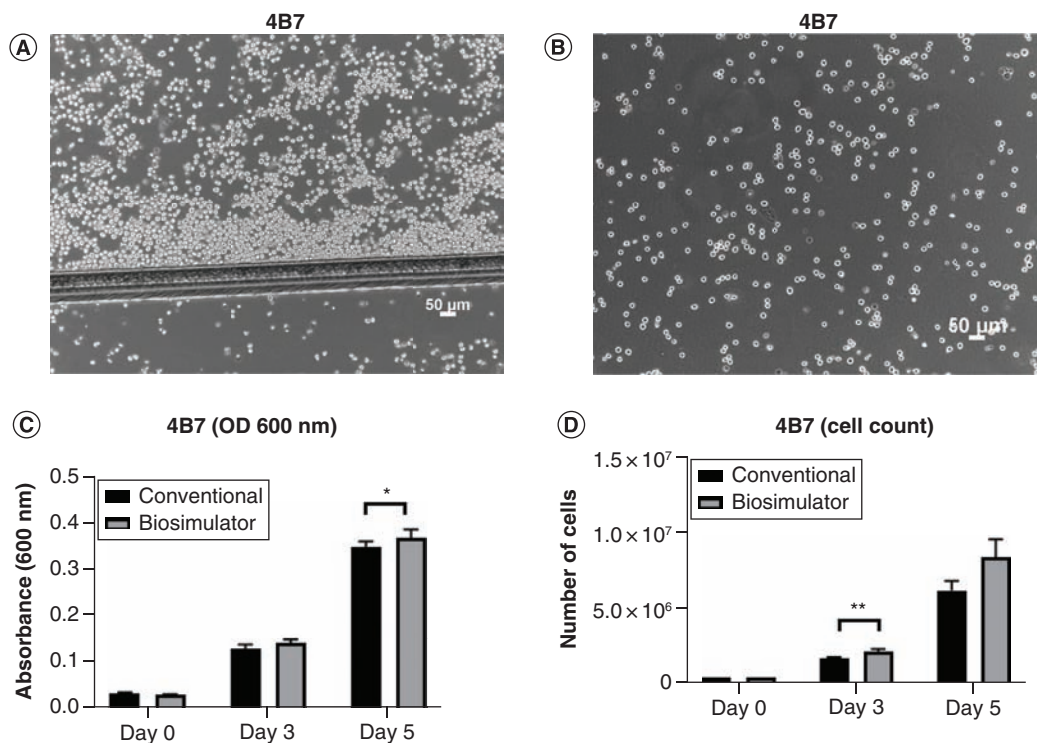


Figure 3. Engraved surface-induced proliferation of the 4B7 nonadherent cells. The hybridoma cell 4B7 was induced to proliferate by the engraved surface. (A) Photomicrograph showing 4B7 cells adhering to the engraving of a biosimulator compared with (B) growth in a conventional dish. (C) Absorbance at 600 nm of 4B7 cells growing in a biosimulator or conventional dish. (D) Cell count of 4B7 cells growing in a biosimulator or conventional dish using a hemocytometer.

* $p < 0.05$, ** $p < 0.01$ as determined by *t*-test.

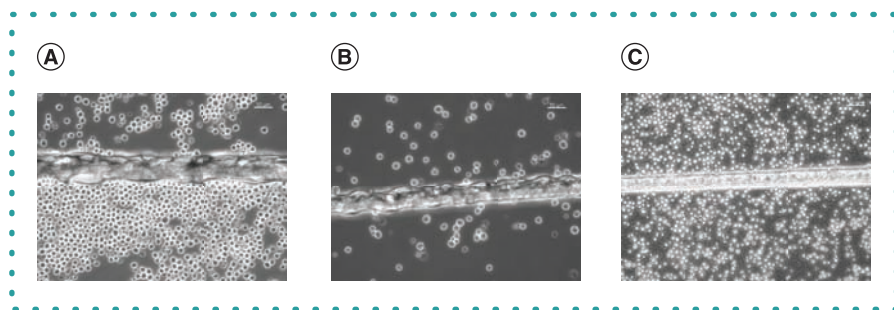


Figure 4. Treatment of nonadherent 4B7 cells with specific inhibitors prevented adhesion of cells to the engraved plastic surface. (A) Nonadherent cells adhering to the engraved plastic surface. (B) Salicylic acid treatment prevented adhesion of the nonadherent cells in an engraved plastic dish. (C) Treatment with pectasol prevented cell adhesion in an engraved plastic dish. Experiments were repeated three times.

Culturing the microbiome of air from the built environment (office) using a biosimulator led to the proliferation of the genera *Comamonas*, *Aeromonas*, *Bacillus*, *Clostridium (sensu stricto)*, *Shigella*, *Escherichia*, *Klebsiella*, *Providencia*, *Serratia*, *Exiguobacterium*, *Acinetobacter*, *Neisseria*, *Lysinibacillus*, *Pseudomonas*, *Shewanella*, *Lactococcus* and *Streptococcus*. However, these microorganisms were not observed when cultured by conventional techniques.

Culturing the microbiome of spring water using a biosimulator led to the proliferation of the genus *Proteus*. Culturing the microbiome of soil using a biosimulator led to the proliferation of the genus *Comamonas*.

The principle of contact guidance or topographic guidance was introduced by Ross Harrison in 1914 [10] and refined by Paul Weiss in 1945, when he demonstrated that cells elongate along the direction of the groove and that migration is influenced by the grooves [11]. The cultured cells exhibit thigmotaxis, sensing the surface topography of their environment and reacting to these surface cues.

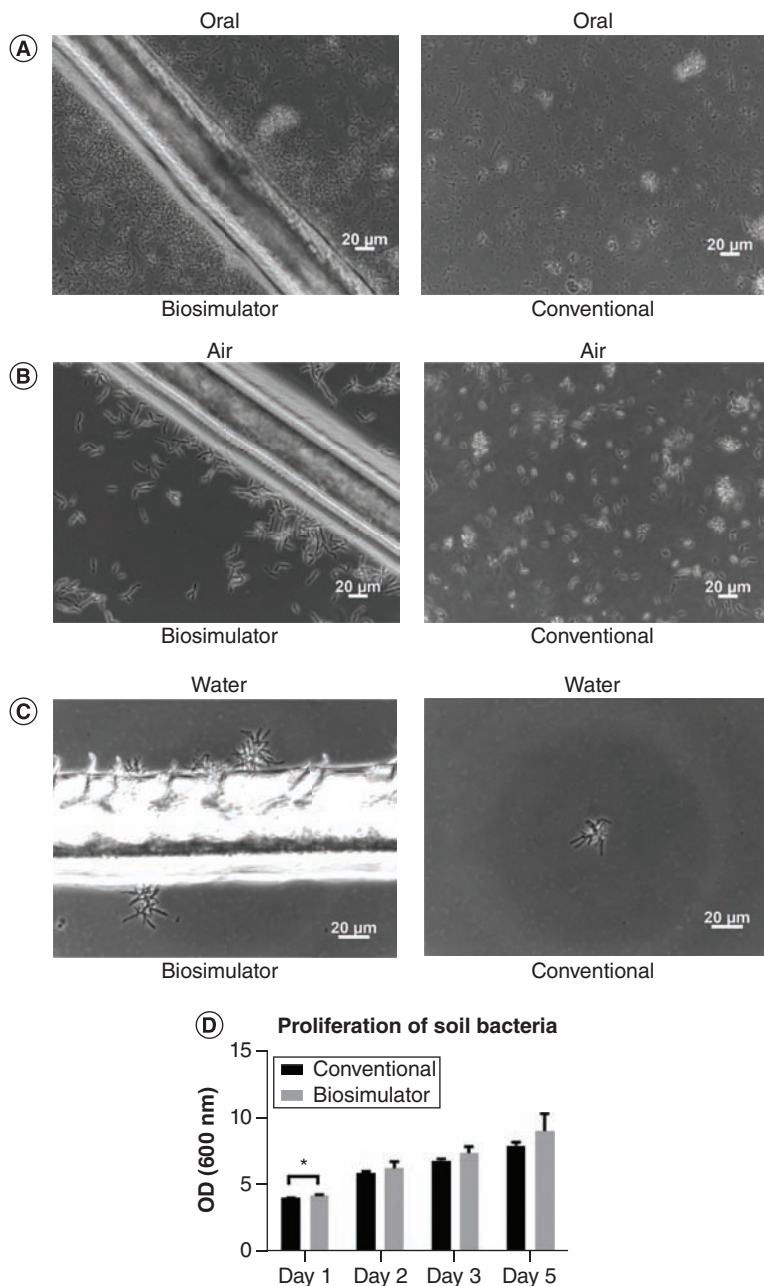


Figure 5. The biosimulator induced proliferation of bacteria from the oral cavity, air, water and soil samples. The engraving in the biosimulator induced proliferation of the bacteria from the (A) oral cavity, (B) air, (C) water and (D) soil samples. Experiments were repeated three times.

Cellular behavior, including cell shape, adhesion, orientation, migration and proliferation, is influenced by surface chemistry and surface topography [12,13].

During cell culture, cells attach to the surface via focal adhesions that connect the surface to the cytoskeleton. The surface chemistry, electrostatic charge, wettability and elastic modulus influence cell growth. The topographical surface provides clues to cell alignment, migration and outgrowth of neurites along a specific orientation. In cell biology studies, to understand the ability of cells to respond to surface topography, grooved substrates are often used. The cells are physically guided along the direction of the grooves, reorganized by the cytoskeleton. However, the mechanism by which cells recognize surface geometry is not clearly understood. The literature suggests it may be a passive process, whereby adhesion molecules best fitting the local topography simply draw cells or cellular components into the observed shape. In several cell lines, surface topography has been shown to be important for the early events of attachment and formation of focal adhesions, activating mechanotransduction events which may eventually determine cell fate and consequent

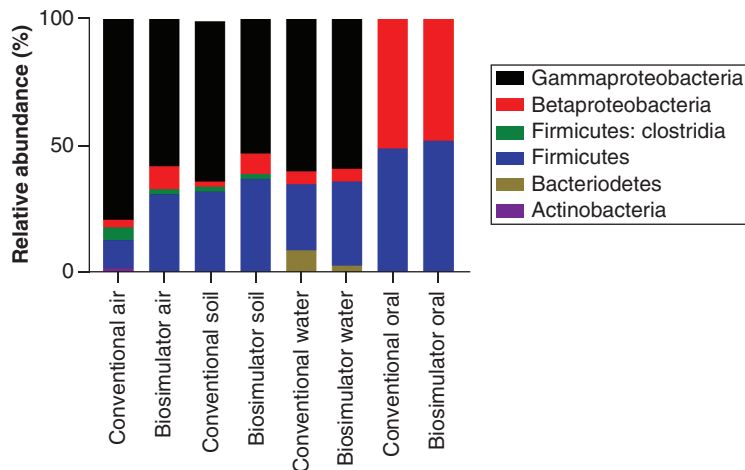


Figure 6. Relative abundance of bacteria at the phylum level cultured in the biosimulator or conventional dishes. Bacteria from air, soil, water and oral cavity samples were cultured in a biosimulator or conventional dish and the taxonomy determined by 16S rRNA sequencing. Each bar represents the mean of three samples.

tissue formation. Among different topographies, micrometer-sized grooved surfaces have been extensively studied for their effects on cell alignment because they can be easily fabricated. As an example, culture of osteogenic cells on grooved surfaces results in strong orientation in the direction of the grooves – unlike on flat surfaces, where a random orientation is generally observed. It has also been demonstrated that microgrooves with widths similar to the cell size induce better cell guidance, whereas the guidance is weaker when cells are cultured in grooves with widths larger than the cells [14–16]. Focal adhesions and actin microfilament bundles and microtubules are found to align along micrometer-sized grooves and ridges, whereas, on smooth substrates, no preferred orientation is exhibited by cells and cytoskeletal elements [17]. In the culture of osteoblastic cells on microgrooves with widths ranging from 4 to 38 μm , it was shown that the narrower grooves (4–16 μm ; 0.5–2 \times cell size) are more effective in guiding the cell orientation. Similarly, it was shown that microgrooves with widths ranging from 2 to 12 μm exhibit great contact guidance effects on the shape and orientation of rat bone marrow cells and fibroblasts [16].

Knowledge of the phenomenon that cells have affinity for grooves on the substrate has led to the development of the field of cellular micropatterning. Cellular micropatterning is a tool to accurately design cell–substrate attachment, tissue engineering, biological assays and biosensors, and is used for drug development studies [18]. A broad range of techniques and materials have been employed to fabricate well-defined topographical and chemical cues to assess cell micropatterning. Some of these fabrication techniques are based on photolithography and reactive ion etching that may be followed by anisotropic etching [19]. In recent years, microfluidics encompassing sophisticated micropatterning designs has led to the development of powerful tools for single cell analysis. The localized microenvironment is precisely controlled by microfluidic techniques, thereby increasing accuracy. The technique is important for disease diagnosis and personalized medicine [20].

Micropatterning can be fabricated into microwell arrays to achieve three different dimensions: single cell (1D), cell monolayer (2D) and cell spheroid (3D). As cells in the *in vivo* environment are surrounded by other cells in three dimensions, 2D cell culture does not adequately take into account the natural environment of cells. As a result, 2D cell culture tests sometimes provide misleading and non-predictive data for *in vivo* responses [21]. 3D *in vitro* cell models provide a more realistic cellular environment and permit the reproduction of *in vivo* cellular phenotypes [22]. Spheroids realistically reflect *in vivo* cell behaviors and provide results more closely aligned to those of *in vivo* tests, thereby making them useful in drug developmental studies [21].

3D cell culture is used in stem cell and tumor cell research [23,24]. In 3D cell culture, human embryonic stem cells (hESCs) have the potential to differentiate into over 200 diversely functioning cell types. Microwell culture permits generation of hESC colonies with a defined size that can later form monodisperse embryoid bodies. When cultured in this system, hESCs retain pluripotency and self-renewal, and can be passaged to standard unconstrained culture conditions [23]. At the intersection between tissue engineering and oncology, 3D *in vitro* tumor models simulate the *in vivo* physiological microenvironment. Working in 3D involves the formation of spheroids – aggregates that can either be grown in suspension, encapsulated, or grown on top of a 3D matrix using different 3D methods [25]. Many cell lines show a reduced proliferation rate in 3D cultures compared with those cultured in 2D. Furthermore, many currently available 3D cell culture techniques are slow, time-consuming, expensive and lack reproducibility [21].

In the initial days of culture in the biosimulator, the pattern of the engraving influenced the nature of cell adherence: the cells were more adhered on the outer edge of the engraved line than the inner edge. It is not understood why the cells show polarity when cultured

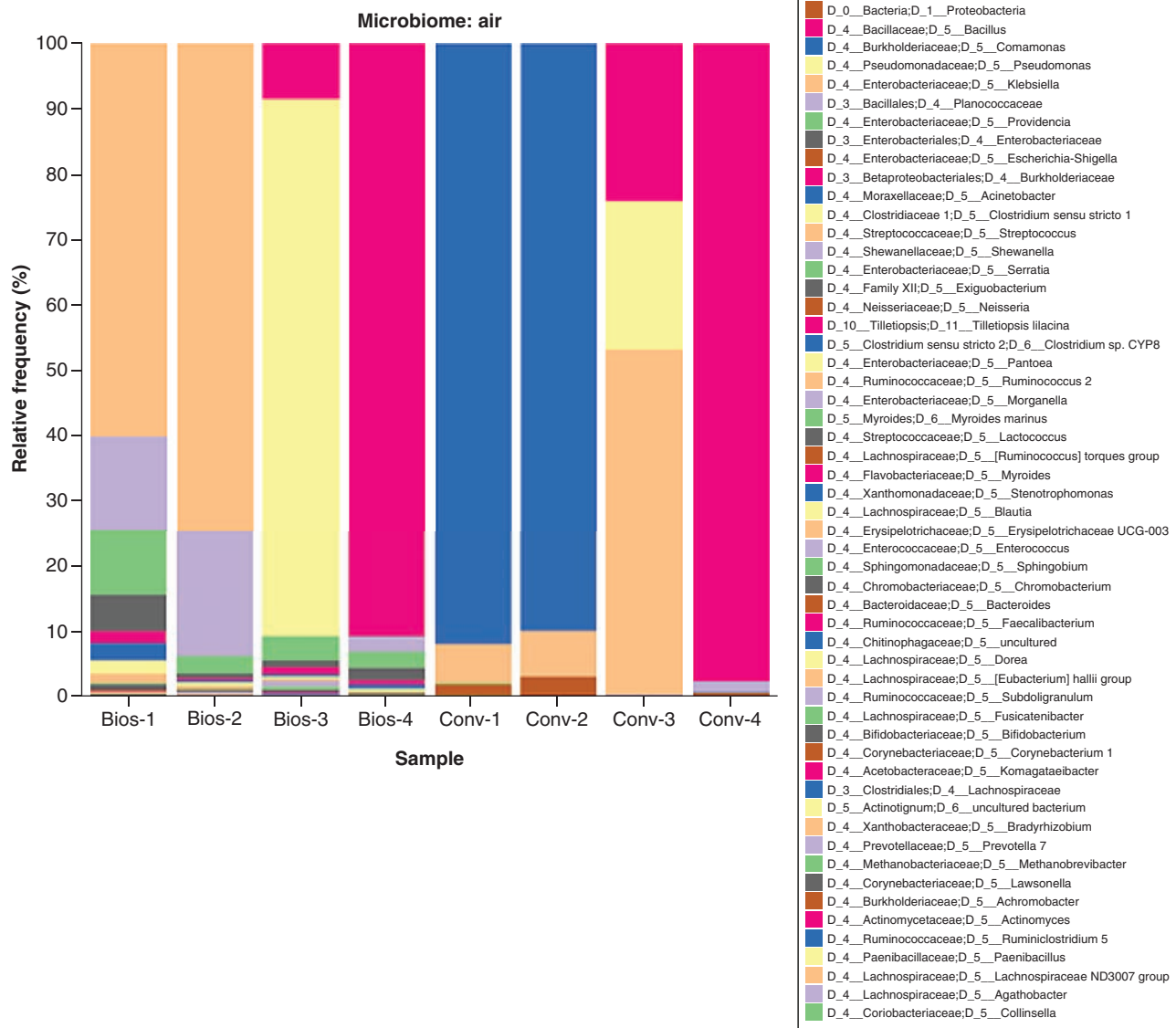
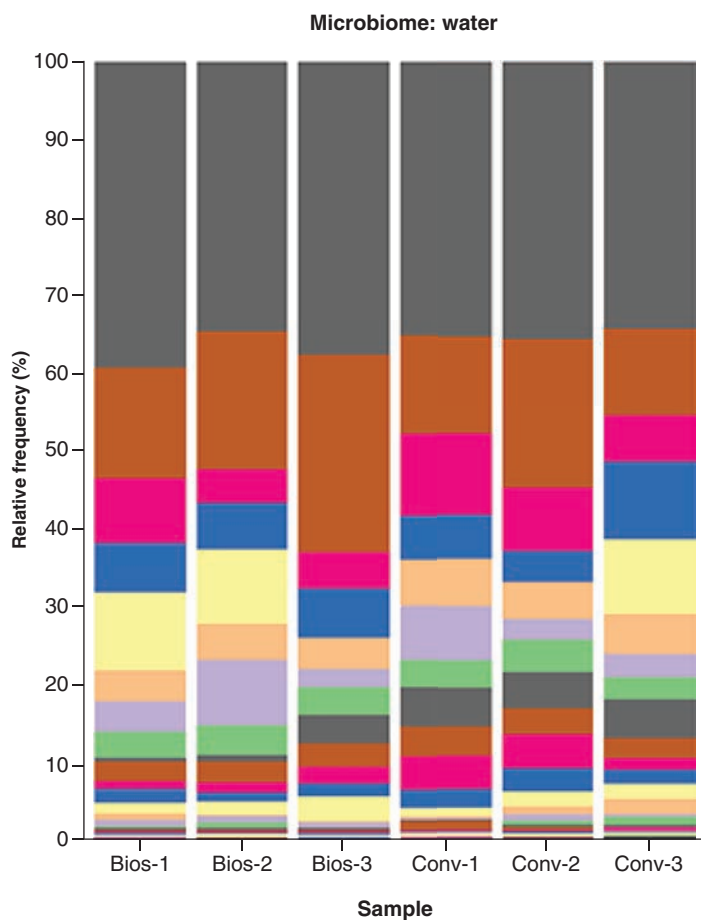


Figure 7. Relative abundance of microorganisms of air (bacteria and fungi) at the genus level cultured in the biosimulator or conventional dishes. Bacteria from air (office) were cultured in a biosimulator or conventional dish for 48 h and the taxonomy determined by 16S rRNA sequencing (n = 4 per treatment).

on a dish with parallel engravings; however, the physical features influencing the cells to form patterns include the circular shape of the Petri dish and the engravings on the hydrophilic plastic surface.

The engraving on the plastic surface did not induce very strong affinity to the cells, which had only a weak adhesion to the engravings. Rapid shaking and extreme washing prevented adhesion of the nonadherent cells. Nevertheless, the adhesion induced proliferation of eukaryotic and prokaryotic cells.

The fundamental units of cell adhesion are protein complexes consisting of three classes of proteins: cell adhesion molecules/adhesion receptors, extracellular matrix proteins and cytoplasmic plaque/peripheral membrane proteins. The cell adhesion proteins include members of the integrin, cadherin, immunoglobulin, selectin and proteoglycan super families [26]. We have not deter-



- D_4__Aeromonadaceae;D_5__Aeromonas
- D_4__Bacillaceae;D_5__Bacillus
- D_4__Planococcaceae;D_5__Lysinibacillus
- D_4__Enterobacteriaceae;D_5__Providencia
- D_3__Bacillales;D_4__Planococcaceae
- D_4__Enterobacteriaceae;D_5__Klebsiella
- D_4__Burkholderiaceae;D_5__Comamonas
- D_3__Enterobacteriales;D_4__Enterobacteriaceae
- D_5__Myroides;D_6__Myroides marinus
- D_4__Moraxellaceae;D_5__Acinetobacter
- D_4__Flavobacteriaceae;D_5__Myroides
- D_3__Betaproteobacteriales;D_4__Burkholderiaceae
- D_4__Pseudomonadaceae;D_5__Pseudomonas
- D_4__Shewanellaceae;D_5__Shewanella
- D_4__Family XII;D_5__Exiguobacterium
- D_4__Enterococcaceae;D_5__Vagococcus
- D_4__Enterobacteriaceae;D_5__Pantoea
- D_5__Myroides;D_6__Myroides sp. OTU s6b
- D_4__Enterobacteriaceae;D_5__Morganella
- D_4__Enterobacteriaceae;D_5__Serratia
- D_4__Streptococcaceae;D_5__Lactococcus
- D_4__Enterobacteriaceae;D_5__Escherichia-Shigella
- D_4__Xanthomonadaceae;D_5__Stenotrophomonas
- D_4__Enterococaceae;D_5__Enterococcus
- D_2__Bacilli;D_3__Bacillales
- D_4__enterobacteriaceae;D_5__Proteus
- D_4__Chromobacteriaceae;D_5__Chromobacterium
- D_4__Weeksellaceae;D_5__Chryseobacterium
- D_4__Vibrionaceae;D_5__Vibrio
- D_4__Hydrogenophilaceae;D_5__Thiobacillus
- D_4__Enterobacteriaceae;D_5__Hafnia-Obesumbacterium
- D_4__Weeksellaceae;D_5__Empedobacter
- D_4__Corynebacteriaceae;D_5__Lawsonella
- D_5__Joenoides;D_6__Joenoides intermedia
- D_5__Paenibacillus;D_6__Paenibacillus taiwanensis
- D_4__Clostridiaceae 1;D_5__Clostridium sensu stricto 1
- D_4__Neisseriaceae;D_5__Neisseria
- D_4__Sphingobacteriaceae;D_5__Sphingobacterium
- D_5__Paenibacillus;D_6__Paenibacillus sp. St-s
- D_5__Empedobacter;D_6__Empedobacter sp. PH7-1
- D_5__uncultured;D_6__bacterium DCE29
- D_3__Lactobacillales;D_4__Enterococcaceae
- DD_4__Nitrosomonadaceae;D_5__MND1
- D_4__Burkholderiaceae;D_5__Alcaligenes
- D_5__Microcoleus PCC-7113;D_6__Microcoleus sp. HTT-U-KK5
- D_4__Propionibacteriaceae;D_5__Cutibacterium
- D_4__Chromobacteriaceae;D_5__Vogesella
- D_0__Bacteria;__

Figure 8. Relative abundance of microorganisms of water at the genus level cultured in the biosimulator or conventional dishes. Bacteria from spring water were cultured in a biosimulator or conventional dish for 48 h and the taxonomy determined by 16S rRNA sequencing (n = 3 per treatment).

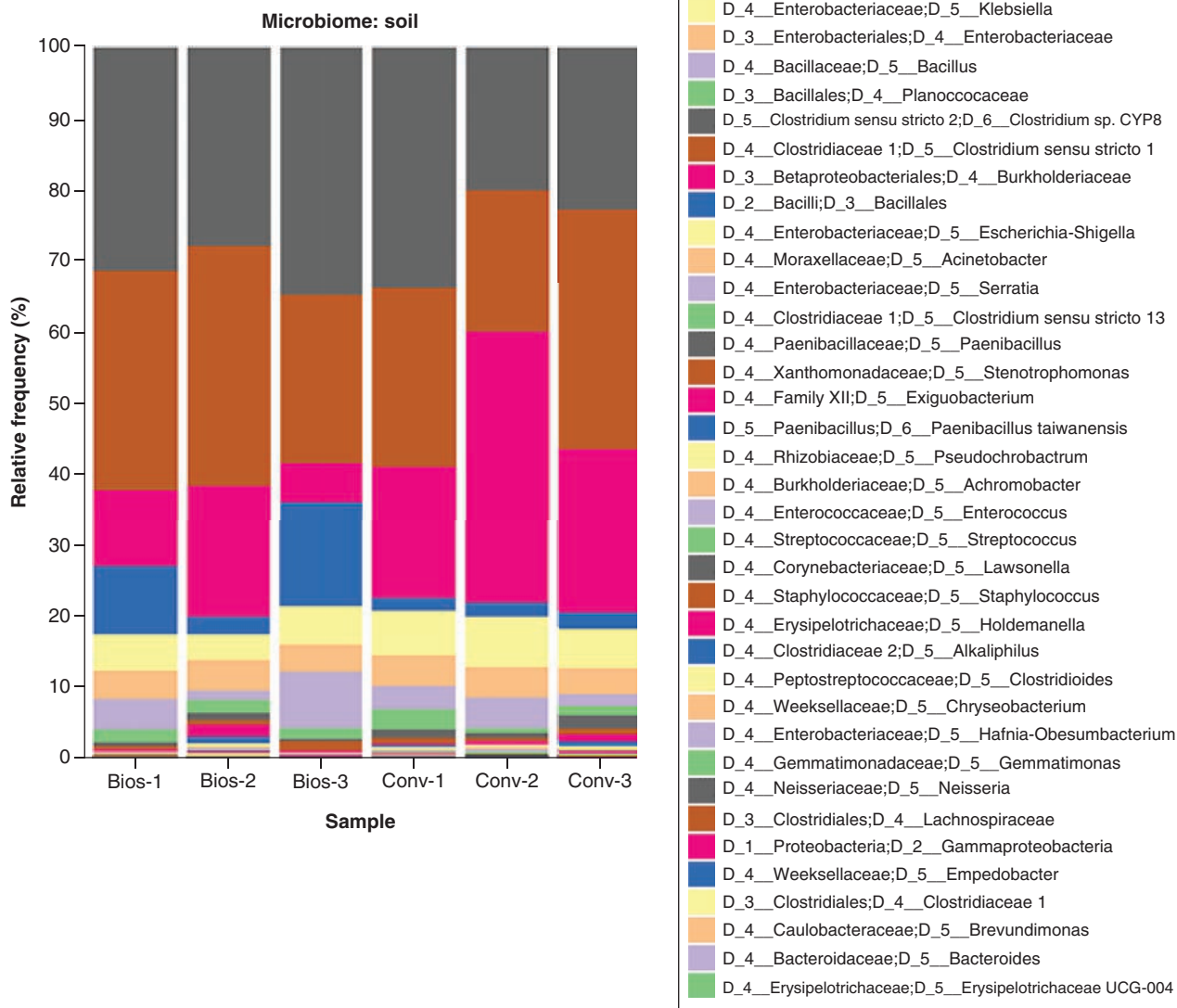


Figure 9. Relative abundance of microorganisms of soil at the genus level cultured in the biosimulator or conventional dishes. Bacteria from soil were cultured in a biosimulator or conventional dish for 48 h and the taxonomy determined by 16S rRNA sequencing (n = 3 per treatment).

mined which adhesion molecules were expressed on the nonadherent cells when cultured in a biosimulator. However, we determined whether inhibiting the expression of the adherent proteins would prevent the nonadherent cells from adhering to the engraving.

For these inhibition studies, we used salicylic acid and pectasol. It is known that salicylic acid prevents adhesion of eukaryotic and microbial cells [27–31]. The adhesion is mediated by ERK signaling and the inhibition of this signaling prevents adhesion [32,33]. For example, coating urinary catheters with salicylic acid reduces bacterial adherence and the risk of urinary tract infection [30].

Pectasol-C is a modified pectin compound used in the inhibition of adhesion and metastasis in cancer cells [6]. Galectin-3 (Gal-3) is a 29-kDa β -galactoside-binding adhesion protein and is expressed intracellularly and extracellularly by various cell types. Pectasol is known to inhibit Gal-3, thereby inhibiting adhesion [34]. In this study, we used both salicylic acid and pectasol for inhibition studies. The cells did not adhere to the engravings of the biosimulator in the presence of salicylic acid and pectasol, demonstrating that the adhesion was mediated by adhesion proteins.

Biofouling is a limiting factor in medical devices. When associated with the biological environment, biomedical devices are prone to surface biofouling due to adhesion of microbial or thrombotic agents [35]. We demonstrated that engravings could predict where

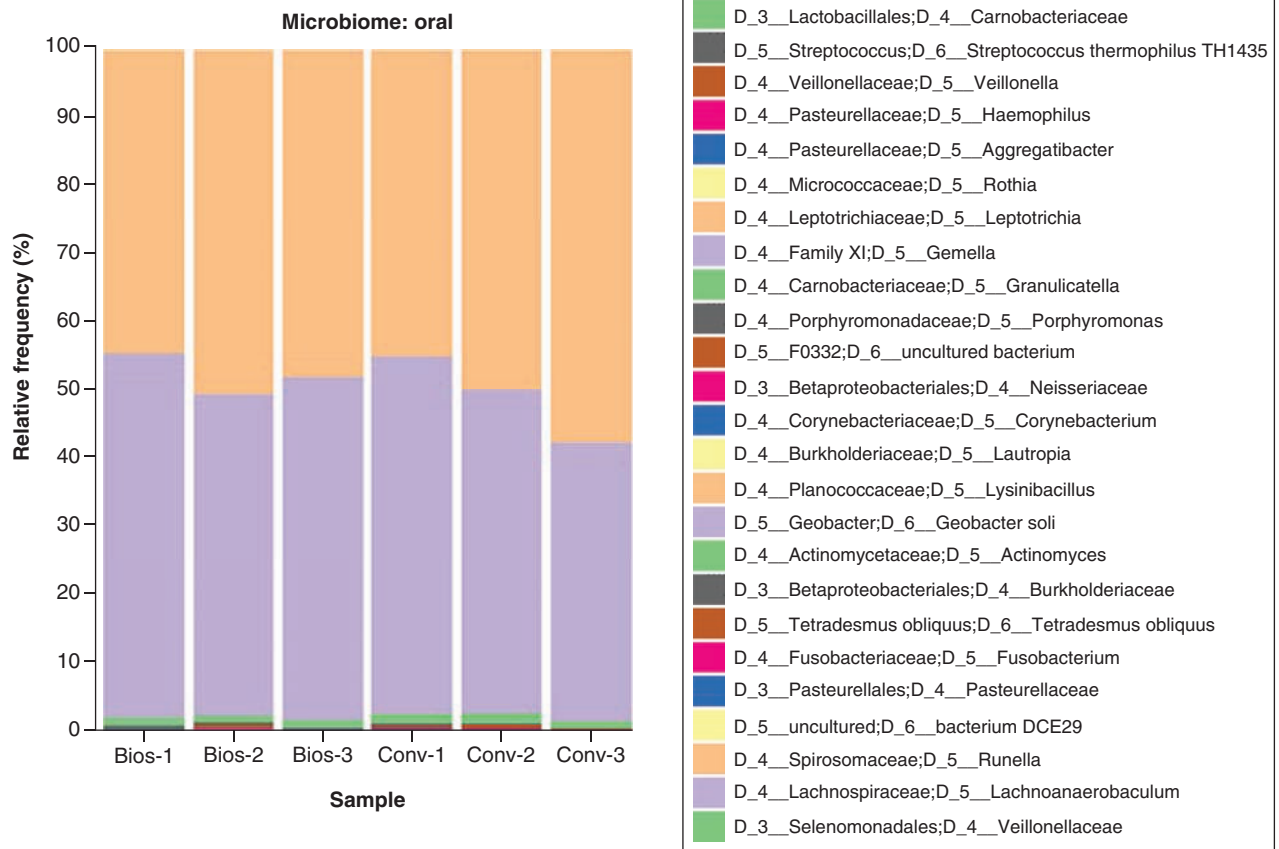


Figure 10. Relative abundance of microorganisms of the oral cavity at the genus level cultured in the biosimulator or conventional dishes. Bacteria from the oral cavity were cultured in a biosimulator or conventional dish for 48 h and the taxonomy determined by 16S rRNA sequencing (n = 3 per treatment).

nonadherent cells adhere. Based on this property, we could design better probes for biomedical applications that could resist biofouling. The phenomenon thus has wide applications in biomedical engineering.

Use of animal models is the preferred method for drug development studies, and single cell analysis provides key information critical to understanding disease processes. However, animal models are expensive and cumbersome, and the researcher has to analyze and collect data of single cells from a pool of cells. Current strategies do not allow analysis of single cells without removing them from the context of interest, which not only destroys contextual information but also may impair the process under study [36]. The induction of adherence in nonadherent cells has wide application in cell biology. The phenomenon could be used to study the mechanism by which autoreactive T cells adhere to pancreatic β cells. Similarly, the mechanism by which monocytes or macrophages adhere to artery walls could be studied using a biosimulator. We have demonstrated that pattern formation can be prevented using drugs that prevent cell adhesion. Based on this principle, new drugs could be tested for their ability to prevent adhesion in different cells. Promising drug candidates that inhibit adhesion molecules in autoreactive T cells could help to combat diseases such as Type I diabetes. Use of the biosimulator to aid development of novel drugs by inhibiting adhesion of nonadherent cells is a more cost-effective strategy than using animal models.

The majority of microorganisms found in nature, including pathogens infecting humans, animals and plants, are nonculturable using conventional techniques [37]. A device that could be used to induce proliferation of these microorganisms will be beneficial in diagnostics as well as the development of new drugs and vaccines.

There have been few modifications in the design and construction of the Petri dish since its development in the 19th century by the German bacteriologist Julius Petri. Surface modified (hydrophilic) polystyrene plates are in vogue for cell culture studies. When adherent cells are cultured on a Petri dish, they spread rapidly and grow to confluence within a couple of days (the exact time required to form confluence depends on the nature of the cell line). However, when nonadherent cells are cultured, some cells attach to the bottom of

the Petri dish, but the majority remain suspended in the medium. Currently, there are no specialized plates for transforming nonadherent cells to adherent cells.

In this paper, it is demonstrated that the biosimulator is a 2D cell system. Most of the 2D systems in the literature are designed for adherent cells; we developed the biosimulator for nonadherent cells and the microbiome. The biosimulator does not have any special coating for inducing adherence. The only variable is the engraving that induces adhesion and proliferation of eukaryotic cells and the microbiome. The width of the engraving is larger than the nonadherent cells. Unlike the adherent cells that formed lamellopodia in the grooves, there was no lamellopodia formation in the nonadherent cells attached to the engravings, resulting in weak affinity of the cells to the engravings. The purpose of the biosimulator is to induce adhesion of nonadherent cells so that they could be used for drug developmental studies; however, further work is required to determine whether induction of adhesion by the biosimulator changes the properties of the nonadherent cells. In addition to induction of adhesion in nonadherent cells, the biosimulator also induced adhesion of microorganisms, and thus could also be used to monitor the microbiome of host and environmental samples.

We used the biosimulator to induce proliferation of microorganisms from different environments: air, water, soil and host. The microorganisms from the environmental samples proliferated within 24 h in a biosimulator. In the first 24 h, we observed that the bacteria had more affinity to the engraving; after 24 h the whole biosimulator was covered with bacteria. To determine if there were changes in the microbial species after culture in different conditions, we cultured the environmental samples in a biosimulator as well as a conventional Petri dish. Microbial sequencing demonstrated that the biosimulator could induce proliferation of microorganisms better than culturing in conventional dishes; we observed several species of bacteria in the environmental samples cultured in a biosimulator that were not seen in those cultured in conventional dishes. We hypothesize that the biosimulator may be useful in encouraging the proliferation of difficult-to-culture microorganisms.

To conclude, the induction of adhesion and proliferation of nonadherent cells and microorganisms on an engraved plastic surface will open new avenues of research in immunology, cell biology and microbiology.

Supplementary data

To view the supplementary data that accompany this paper please visit the journal website at: www.future-science.com/doi/suppl/10.2144/btn-2020-0022

Author contributions

S Thomas conceived, designed and performed the experiments, analyzed the data, and wrote the paper.

Acknowledgments

The author thanks MA Azcarate-Peril and J Roach of the University of North Carolina Microbiome Core for microbiome analysis.

Financial & competing interests disclosure

The author wishes to acknowledge receiving grants and support from the Wawa Foundation, Abraham Thomas Foundation and Women's Board of Lankenau. The UNC Microbiome Core is funded partially by NIH/NIDDK grant number P30 DK34987. The author has no other relevant affiliations or financial involvement with any organization or entity with a financial interest in or financial conflict with the subject matter or materials discussed in the manuscript apart from those disclosed.

No writing assistance was utilized in the production of this manuscript.

Open access

This work is licensed under the Attribution-NonCommercial-NoDerivatives 4.0 Unported License. To view a copy of this license, visit <http://creativecommons.org/licenses/by-nc-nd/4.0/>

References

1. Wu CY, Stoecklein D, Kommajosula A *et al*. Shaped 3D microcarriers for adherent cell culture and analysis. *Microsyst. Nanoeng.* 4, 21 (2018).
2. Barcina I, Arana I. The viable but nonculturable phenotype: a crossroads in the life-cycle of non-differentiating bacteria? *Rev. Environ. Sci. Biotechnol.* 8, 245–255 (2009).
3. Li L, Mendis N, Trigui H, Oliver JD, Faucher SP. The importance of the viable but nonculturable state in human bacterial pathogens. *Front. Microbiol.* 5, 258 (2014).
4. Caporaso JG, Lauber CL, Walters WA, Berg-Lyons D *et al*. Global patterns of 16S rRNA diversity at a depth of millions of sequences per sample. *Proc. Natl Acad. Sci. USA* 108, 4516–4522 (2011).
5. Cao Y, DuBois DC, Almon RR, Jusko WJ. Pharmacokinetics of salsalate and salicylic acid in normal and diabetic rats. *Biopharm. Drug Dispos.* 33, 285–291 (2012).
6. Jiang J, Eliaz I, Sliva D. Synergistic and additive effects of modified citrus pectin with two polybotanical compounds, in the suppression of invasive behavior of human breast and prostate cancer cells. *Integr. Cancer Ther.* 12, 145–152 (2013).
7. Thomas S, Izard J, Walsh E *et al*. The host microbiome regulates and maintains human health: a primer and perspective for non-microbiologists. *Cancer Res.* 77, 1783–1812 (2017).
8. Wells CL, Wilkins TD. Clostridia: Spore forming anaerobic Bacilli (Chapter 18). In: *Medical Microbiology. (4th Edition)*. Baron S Ed.). University of Texas Medical Branch at Galveston, Galveston, TX (1996).
9. Dewhirst FE, Chen T, Izard J, Paster BJ *et al*. The human oral microbiome. *J. Bacteriol.* 192, 5002–5017 (2010).
10. Harrison RG. The reaction of embryonic cells to solid structures. *J. Exp. Zool.* 17, 521–544 (1914).
11. Weiss P. Experiments on cell and axon orientation *in vitro*: the role of colloidal exudates in tissue organization. *J. Exp. Zool.* 100, 353–386 (1945).

12. Hamilton DW, Oakley C, Jaeger NA, Brunette DM. Directional change produced by perpendicularly-oriented microgrooves is microtubule-dependent for fibroblasts and epithelium. *Cell Motil. Cytoskeleton* 66, 260–271 (2009).
13. Li Q, Guo Y, Wang Y. The influence of microgrooved surfaces on the behavior and cellular function of osteoblasts. *Dent. Oral Craniofac. Res.* 2. doi: 10.15761/DOCR.1000176 (2016) (Epub ahead of print).
14. Zhou F, Yuan L, Huang H, Chen H. Phenomenon of “contact guidance” on the surface with nano-micro-groove-like pattern and cell physiological effects. *Chin. Sci. Bull.* 54, 3200–3205 (2009).
15. Peterbauer T, Yakunin S, Siegel J *et al.* Dynamics of spreading and alignment of cells cultured *in vitro* on a grooved polymer surface. *J. Nanomater.* 2011 Article ID: 413079 (2011).
16. Sun L, Pereira D, Wang Q *et al.* Controlling growth and osteogenic differentiation of osteoblasts on microgrooved polystyrene surfaces. *PLoS ONE* 11(8), e0161466 (2016).
17. Teixeira AI, Abrams GA, Bertics PJ, Murphy CJ, Nealey PF. Epithelial contact guidance on well-defined micro- and nanostructured substrates. *J. Cell Sci.* 116(Pt 10), 1881–1892 (2003).
18. Tourovskaia A, Barber T, Wickes BT *et al.* Micropatterns of chemisorbed cell adhesion-repellent films using oxygen plasma etching and elastomeric masks. *Langmuir* 19, 4754–4764 (2003).
19. Fernández-Castillejo S, Formentín P, Catalán Ú, Pallarès J, Marsal LF, Solà R. Silicon microgrooves for contact guidance of human aortic endothelial cells. *Beilstein J. Nanotechnol.* 8, 675–681 (2017).
20. Gao D, Jin F, Zhou M, Jiang Y. Recent advances in single cell manipulation and biochemical analysis on microfluidics. *Analyst* 144, 766–781 (2019).
21. Edmondson R, Broglie JJ, Adcock AF, Yang L. Three-dimensional cell culture systems and their applications in drug discovery and cell-based biosensors. *Assay Drug Dev. Technol.* 12, 207–218 (2014).
22. Park J, Müller M, Kim J, Seidel H. Fabrication of a cell-adhesive microwell array for 3-dimensional *in vitro* cell model. *Biomed. Eng. Lett.* 5, 140–146 (2015).
23. Mohr JC, de Pablo JJ, Palecek SP. 3-D microwell culture of human embryonic stem cells. *Biomaterials* 27, 6032–6042 (2006).
24. Lv D, Hu Z, Lu L, Lu H, Xu X. Three-dimensional cell culture: a powerful tool in tumor research and drug discovery. *Oncol. Lett.* 14, 6999–7010 (2017).
25. Hoarau-Véchet J, Rafii A, Touboul C, Pasquier J. Halfway between 2D and animal models: are 3D cultures the ideal tool to study cancer-microenvironment interactions? *Int. J. Mol. Sci.* 19(1), pii: E181 (2018).
26. Gumbiner BM. Cell adhesion: the molecular basis of tissue architecture and morphogenesis. *Cell* 84, 345–357 (1996).
27. Gerli R, Gresele P, Bistoni O *et al.* Salicylates inhibit T cell adhesion on endothelium under nonstatic conditions: induction of L-selectin shedding by a tyrosine kinase-dependent mechanism. *J. Immunol.* 166, 832–840 (2001).
28. Eisele G, Schwedhelm E, Schieffer B, Tsikas D, Boger RH. Acetylsalicylic acid inhibits monocyte adhesion to endothelial cells by an antioxidative mechanism. *J. Cardiovasc. Pharmacol.* 43, 514–521 (2004).
29. Weber C, Erl W, Pietsch A, Weber PC. Aspirin inhibits nuclear factor-kappa B mobilization and monocyte adhesion in stimulated human endothelial cells. *Circulation* 91, 1914–1917 (1995).
30. Farber BF, Wolff AG. The use of salicylic acid to prevent the adherence of *Escherichia coli* to silastic catheters. *J. Urol.* 149, 667–670 (1993).
31. Bandara BM, Sankaridurg PR, Willcox MD. Non-steroidal anti inflammatory agents decrease bacterial colonisation of contact lenses and prevent adhesion to human corneal epithelial cells. *Curr. Eye Res.* 29, 245–251 (2004).
32. Pillinger MH, Capodici C, Rosenthal P *et al.* Modes of action of aspirin-like drugs: salicylates inhibit erk activation and integrin-dependent neutrophil adhesion. *Proc. Natl Acad. Sci. USA* 95, 14540–14545 (1998).
33. Tanimura S, Takeda K. ERK signalling as a regulator of cell motility. *J. Biochem.* 162, 145–154 (2017).
34. Hossein G, Keshavarz M, Ahmadi S, Naderi N. Synergistic effects of PectaSol-C modified citrus pectin an inhibitor of Galectin-3 and paclitaxel on apoptosis of human SKOV-3 ovarian cancer cells. *Asian Pac. J. Cancer Prev.* 14, 7561–7568 (2013).
35. Harding JL, Reynolds MM. Combating medical device fouling. *Trends Biotech.* 32, 140–146 (2014).
36. Sarkar A, Koltz S, Lauffenburger DA, Han J. Microfluidic probe for single-cell analysis in adherent tissue culture. *Nature Commun.* 5, 3421 (2014).
37. Stewart EJ. Growing unculturable bacteria. *J. Bacteriol.* 194, 4151–4160 (2012).

Contact us

Editorial Department

Senior Editor

Abigail Sawyer

asawyer@biotechniques.com

Business Development and Support

Commercial Director

Sarah Mayes

s.mayes@future-science-group.com



[@MyBioTechniques](https://twitter.com/MyBioTechniques)



[@biotechniques](https://www.facebook.com/biotechniques)



[BioTechniques](https://www.linkedin.com/company/biotechniques)